Soft Matter

Accepted Manuscript

This article can be cited before page numbers have been issued, to do this please use: B. Viada, C. I. Cámara and L. M. Yudi, *Soft Matter*, 2019, DOI: 10.1039/C8SM02301H.

ROYAL SOCIETY OF CHEMISTRY

rsc.li/soft-matter-journal

View Article Online
DOI: 10.1039/C8SM02301H
Second Revision – SM-ART-11-2018-002301.R1

Destabilizing effect of perfluorodecanoic acid on simple membrane models

Benjamín Viada[1,2], Candelaria I. Camara*[1,2], Lidia M. Yudi*[1,2]

[1] Universidad Nacional de Córdoba. Facultad de Ciencias Químicas. Departamento de Fisicoquímica. Córdoba. Argentina.

[2] Consejo Nacional de Investigaciones Científicas y Técnicas, CONICET. Instituto de Investigaciones en Fisicoquímica de Córdoba, INFIQC. Córdoba. Argentina.

Corresponding authors: Lidia M.Yudi: mjudi@fcq.unc.edu.ar

Candelaria I. Cámara: ccamara@fcq.unc.edu.ar

Abstract

Perfluoroalkyl acids (PFA) are amphiphilic surfactants widely used in industry with several commercial applications. An important feature of these compounds is their non-biodegradability and the tendency to bio-accumulate in the environment, which made these compounds to be considered among the most persistent pollutants worldwide. Many articles evidence their toxic effect on humans and wildlife. For this reason, more and more efforts have been made to better understand the effect of these compounds on living organisms. The aim of the present study is to understand how electrostatic interactions and film compactness of biological membranes models modulate their interaction with PFA, more specifically with perfluorodecanoic acid (PFD). Langmuir isotherms and Brewster angle microscopy (BAM) are used to evaluate the effect of PFD on lipid membrane models (air/water monolayers and vesicles) analyzing the behavior of PFD:lipid mixtures. The lipids used in this study are distearoyl phosphatidic acid (DSPA), dilauroyl phosphatidic acid (DLPA) and distearoyl phosphatidylethanolamine (DSPE). PFD induces an increase in the mean molecular area per lipid in monolayers, mainly at lower surface pressures. BAM images demonstrate that PFD mixes with DLPA,

View Article Online
DOI: 10.1039/C8SM02301H
Second Revision – SM-ART-11-2018-002301.R1

inducing a decrease in gray level, while it forms a non-miscible mixture with DSPA segregating PFD domains. Insertion studies of PFD within monolayers and dynamic light scattering experiments demonstrate that PFD can penetrate into monolayers and bilayers above 30 mNm^{-1}, which is the lateral pressure value accepted for cellular bilayer.

Keywords:

Perfluorodecanoic acid

Brewster Angle Microscopy

Phospholipids

Exclusion pressure

Micelles

1. Introduction

Perfluoroalkyl compunds (PFA) are surfactant molecules in which all the H atoms of the hydrocarbon tail are replaced by fluorine atoms[1]. These particular kinds of molecules are widely used in industrial and commercial applications. Some of the most frequent uses are: grease proof textiles with soil repellency and stain resistance, food contact paper, firefighting foams, lubricants, cosmetic and pharmaceutical products, as photographic emulsifier, aviation hydraulic fluid, and insecticide formulations, among others[1-3]. The strength of C-F bond in the structure of PFA confers to this family of surfactants high chemical stability. Considering the environmental impact of these molecules, their high stability is a disadvantage because makes these compounds almost non metabolic and non-biodegradable and, as a consequence of their long half-life times, they prevail in the ambient[2-3] and tend to bioaccumulate in human body[4]. Some evidence of the bioaccumulation and non-degradability is the presence of PFA in the environment[5], in birds and marine mammals[6], in lake sediments[7], in water[8-11], in human urine[4] and blond[12-13], among other samples[14]. In the last decade an important

View Article Online
DOI: 10.1039/C8SM02301H
Second Revision – SM-ART-11-2018-002301.R1

number of publications have reported the study of the toxicity of these compounds on cells[15-17], animals[18-20] and humans[21-24], and demonstrated that the presence of PFA can be related with several disorders as: low birth weight, hyperuricemia, chronic kidney disease, thyroid disease[24] and immunotoxicity[4]. The degree of pollution caused by PFA and related compounds is so harmful that several countries regulate its production.

The toxicity of PFA in the human systems involves different levels: neurotoxicity, liver toxicity and pulmonary toxicity[2], but it is important to take into account that, due to its amphipathic character, the interaction with biological membrane cannot be avoid. Several publications characterized the behavior of PFA at the air/water interface[25-26] and reported the effect of PFA on membrane models, monolayers[27-30] and bilayers[31-32]. Lehmler and Bummer demonstrated that perfluorinated acids partially mixed with DPPC monolayers while the mixture was immiscible in bilayers in gel phase[33]. Moreover, W. Xie et all found that perfluorooctanoic acid (PFO) partitions more efficiently at the fluid phase of a bilayer of dimiristoil phosphatidylcholine (DMPC) and demonstrated the formation of a mixed PFO:lipid micelles[34]. On the other hand M. Paige stated that the partial miscibility and immiscibility properties between perfluoroalkyl molecules and lipids can be used for modulating the topography of mixed film[30].

Due to the high amphipathic character and toxicity of PFA, there is an increasing interest for characterizing the interactions between them and the cell. The aim of the present paper is the study of the effect of perfluorodecanoic acid (PFD) on cellular membrane models. Our objective is to evaluate how the electrical charge at the interface and the compactness of the phospholipid monolayer modulate the interaction of PFD with membranes models. For this purpose, the behavior of mixed monolayers of PFD with DSPA, DLPA and DSPE was evaluated throught Langmuir compression isotherms and Brewster angle microscopy. Also, we present the study related to the ability of PFD to penetrate a pre-formed monolayer and determine several parameters that allow understanding the factors modulating the PFD:Lipid interaction. By last, we show the results of experiments analyzing the effect of PFD on DSPA and DLPA vesicles followed by nephelometry and dynamic light scattering.

View Article Online
DOI: 10.1039/C8SM02301H
Second Revision – SM-ART-11-2018-002301.R1

2. Materials and Methods

2.1. Materials

Phospholipids 1,2-distearoyl-*sn*-glycerol-3-phosphate (DSPA), 1,2-distearoyl-*sn*-glycerol-3-phosphoethanolamine (DSPE), and 1,2-dilauroyl-*sn*-glycerol-3-phosphate (DLPA) were purchased from Avanti Polar Lipids (Alabaster, Al). Perfluorodecanoic acid (PFD) was purchased from Sigma-Aldrich (purity of 98%). The chemical structures of PFD and the lipids are shown in Figure 1.

LiCl (subphase electrolyte) was purchased from Merck (Germany). Chloroform and Methanol were acquired from Sintorgan (Argentine) and Dorwil S.A (Argentine), respectively. All the reactants used were of the highest commercial purity available. The aqueous solutions were prepared with ultra-pure deionized water (with resistivity of 18 MΩ, obtained from a Milli-Q Gradient System, Millipore, Bedford, MA).

The lipid solutions were prepared in chloroform:methanol 2:1 v/v at a concentration value equal to 1.0 mM. PFD concentration was: 6.0 mM in methanol for compression isotherms experiments, 50.0 mM in ultra-pure water for Gibbs adsorption isotherms and 16 μM in ultra-pure water for DLS and nephelometry experiments (PFD cmc: 2.2 mM[35]). The aqueous solution of LiCl, employed as subphase, was 10.0 mM.

2.2. Methods

2.2.1 Monolayers at the air/water interface

View Article Online
DOI: 10.1039/C8SM02301H
Second Revision – SM-ART-11-2018-002301.R1

Compression isotherms were performed with a KSV Langmuir balance (Mini-trough II, Helsinki - Finland), using the Wilhelmy method with a platinum plate. The Lipids:PFD monolayers were formed by spreading each mixture at the surface of a 10.0 mM LiCl subphase, using a Hamilton micro syringe. After spreading, the solvent was allowed to evaporate by 10 min, and then the film was compressed with two barriers at a compression speed of 10 mm.min^{-1} while the automatic measurement of the lateral surface pressure (π) was carried out. The Teflon trough has an effective film area of 364 mm x 75 mm. Before spreading the Lipids:PFD mixtures, the subphase surface was cleaned by sweeping it with the barriers and then removing any surface contaminant by suction from the interface. This procedure was checked by recording an isotherm in the absence of the lipids and verifying a surface pressure value lower than 0.20 mN.m^{-1}.

The molar ratios Lipid (DSPA or DLPA or DSPE):PFD used were 100:0 (pure Lipid), 80:20, 60:40, 20:80 and 0:100 (pure PFD). The Lipid:PFD mixtures used for Langmuir compression isotherm and Brewster angle microscopy (BAM) experiments were prepared just before spreading.

From the compression isotherms, the surface compression modulus Cs^{-1} (mN.m^{-1}) was calculated as:

$$Cs^{-1} = -A\left(\frac{\partial \pi}{\partial A}\right)_T$$

where π is the surface pressure in mN.m^{-1} and *A* is the area per molecule. The uncertainty of surface compression modulus was $\pm$ 10mN.m^{-1}.

During compression, mixed monolayers were observed using Brewster Angle Microscopy (BAM) with an EP3 Imaging Ellipsometer (Accurion) equipped with a 20X objective (Nikon, NA 0.35). Previous to the injection the equipment was calibrated with the clean interface in order to determine the relation between the average gray-level of the images and the reflected light intensity (RP). The gray level (GL)

View Article Online
DOI: 10.1039/C8SM02301H
Second Revision – SM-ART-11-2018-002301.R1

of each images was calculate as the difference between RP and the dark signal (DS, value of reflectivity for clean interface, in the absence of lipid)[36-37]. Then, the gray level of the images was calculated as GL= RP – DS. The average gray-levels (± SD) were calculated from 5 different regions corresponding to each phase in at least 2 images for each condition using ImageJ.

In all the experiments de temperature was controlled with a thermocirculator at 21 °C. This value is lower than the transition temperature for all the lipids studied.

2.2.2 Insertion of PFD in pre-formed monolayers and exclusion pressure determination

Studies concerning to insertion of PFD in pre-formed monolayers were carried out using a mini trough of Volume = 5 mL and constant surface area (A = 15.8 cm^2). The procedure followed in these experiments leads to the typical results shown in Figure 2 (in this case, the successive experimental steps carried out for DSPE monolayers are shown as an example). First, the appropriate volume of the lipid solutions (DSPA, DSPE or DLPA), needed to obtain a surface pressure equal to 15 mN/m was injected at the surface of a 10 mM LiCl subphase (red arrow in Figure 2a). Afterwards, successive injections of PFD solution were made inside the subphase (blue arrows in Figure 2a), and the final pressure values, after 12 min, were determined. Then, the change in surface pressure, after each PFD injection, with respect to the initial pressure ($\Delta\pi_i$ / $mN.m^{-1}$), was plotted as a function of the final PFD concentration (Figure 2 (b)), obtaining an initial increase of $\Delta\pi_i$ and a saturation constant $\Delta\pi_i$ value at high concentrations. This saturation PFD concentration value was chosen for the following step: starting from different initial pressures (reached employing different lipid concentration at the surface), PFD was injected into the subphase at this concentration value (Figure 2 (c)). After this, $\Delta\pi_i$ values obtained from figure 2 (c) at each initial pressure, were plotted as a function of the initial pressure (Figure 2 (d)). From the x-intercept in the last figure, the maximum surface pressure value at witch PFD can penetrate into a pre-formed monolayer (exclusion pressure) was determined (blue arrow in Figure 2 (d)).

View Article Online
DOI: 10.1039/C8SM02301H
Second Revision – SM-ART-11-2018-002301.R1

2.2.3 Size determination and Nephelometry

Large unilamellar vesicles (LUVs) of DSPE, DSPA and DLPA were prepared by generating a uniform lipid film on the wall of a conical glass tube from a chloroform:methanol lipid solution and removing the solvent by evaporation under a N_2 flow. Final traces of solvent were eliminated incubating the lipids in a high-vacumm chamber during 2 h. Afterwards, the lipids were re-suspended in 10mM LiCl aqueous solution, to a final concentration of 0.5 mg/mL. The suspension was subjected to 5 cycles of heating-vortex-cooling, each step during 1 min. The heating process was carried out in a 60°C water bath and the cooling incubation was performed in ice bath. The resulting multilamellar vesicles were extruded 20-times through a 100 µm pore filter (Avanti) at 60°C. Under this condition only LUVs of DLPA and DSPA were obtained [38].

The size determinations were performed by dynamic light scattering (DLS) using a Submicron Particle Sizer (Nicomp TM 380). The average sizes obtained for LUVs were (84±16) nm and (71±13) nm for DLPA and DSPA, respectively.

The stability of DSPA and DLPA LUVs upon PFD addition (detergent effect) was tested through vesicle rupture, adding increasing volumes of a 16 µM PFD solution in LiCl 10mM, to the LUV´s solutions (30µL LUVs + 270 µL of 10mM LiCl). Vesicle rupture was followed through turbidity measurements using nephelometry. The diffracted light depends on the size and amount of diffracting particles, and therefore, a decrease in the detected light is observed upon vesicle rupture [39].

Nephelometry measurements were carried out with a Cary Eclipse spectrofluorometer (Agilent Technologies) equipped with a thermally controlled multi-cuvette holder (21°C), setting the wavelength slit in 5 nm and using a 2 mm path cuvette, the excitation and emission wavelengths were set at 523 nm.

View Article Online
DOI: 10.1039/C8SM02301H
Second Revision – SM-ART-11-2018-002301.R1

The relative turbidity was measured after each addition of PFD solution, and the percent of relative turbidity (% RT) was calculated as $\% \mathrm{RT} = {}^{\mathrm{RT^i}}\!/_{\mathrm{RT^0}} \mathrm{x}\, 100$. The symbol *0* refers to the initial values of turbidity and *i* to those after each addition of PFD solution.

3. Results and Discussion

3.1. Langmuir Isotherms and Brewster Angle Microscopy

Figure 1 shows the chemical structures for the different lipids studied (DSPA, DSPE and DLPA) and for PFD. In the case of DSPA and DLPA the average apparent pKa values are: pKa_1=3.2 and pKa_2=8.3, while the corresponding values for DSPE are: pKa_1 = 2.2 and pKa_2= 10.1 [40]. PFD is a strong acid with pKa= -0.17 [41]. Consequently, at the present working condition of pH = 6, DLPA, DSPA and PFD are mono anions, while DSPE is a zwitterion.

With the aim of evaluating the disrupting effect of PFD on membrane models, Langmuir compression isotherms for different mixtures formed by the lipids (DSPA, DSPE or DLPA) and PFD were recorded, as shown in Figure 3.

3.1.1. Effect of PFD on DSPA monolayers:

Figure 3a shows the surface pressure as a function of the mean molecular area for pure PFD (inset), pure DSPA and mixtures DSPA:PFD at different concentration ratios. It is worth highlighting that in the case of pure DSPA or for all the mixtures lipid:PFD, the mean molecular area of the lipid is always represented in the x-axis. Instead, for pure PFD the trough area is plotted in x-axis, due to the high solubility of PFD in water, which makes it difficult to estimate the number of molecules that remain adsorbed at the surface. On the one hand, the behavior of pure PFD under compression was highly

View Article Online
DOI: 10.1039/C8SM02301H
Second Revision – SM-ART-11-2018-002301.R1

dependent on the amount of PFD injected at the interface. At low surface concentration of PFD a slight decrease in the surface pressure at the beginning of the Langmuir isotherm was observed, this effect is attributed to the solubilization of PFD molecules on the aqueous subphase, similar effect was reported for other perfluoroalkyls [35, 42]. Besides, the maximum surface pressure reached was 15 $mN.m^{-1}$. Then, the isotherm corresponding to PFD can be interpreted considering that these molecules do not form a stable film due to their high solubility in water. This high solubility is supported by the fact that BAM images for PFD monolayers do not show a significant difference on gray level with respect to the clean interface (the gray level range is 0.1 ± 0.3 at all the surface pressures analyzed). On the other side, pure DSPA exhibits a condensed isotherm under compression (Cs^{-1} = 230 $mN.m^{-1}$ at π = 40$mN.m^{-1}$, Figure 4 d), characterized by a collapse area and pressure of 38 $Å^2$ and 52$mN.m^{-1}$, respectively. Brewster angle images (Figure 5a) show a condensed and homogeneous film as previously reported[43].

After characterizing the behavior of pure PFD and DSPA, the mixtures DSPA:PFD were analyzed increasing the PFD molar fraction from 0 to 95% (Figure 3a). As can be observed from the isotherms, increasing amounts of PFD in the mixtures produce an increase in the lift off areas (Figure 3d) and in the mean molecular areas at low pressure values (see Figure 4a, where $\Delta Mma = Mma_{\text{with PFD}} - Mma_{\text{without PFD}}$ vs $\%X_{PFD}$ at π = 20 $mN.m^{-1}$ is plotted), evidencing the presence of PFD in the monolayer. It is worth noting at this point that, as explained above, all the isotherms are related to the area per phospholipid molecule, calculated from the ratio between the total area of the trough, at each point of the compression, and the total number of phospholipid molecules, regardless of whether the injected solution was of pure lipid or lipid:PFD mixture. In this way, an increase in the area per lipid molecule in the presence of PFD can be interpreted either as a higher lipid area within the monolayer or else that the PFD molecules are inserted within the monolayer, occupying a space and resulting in a greater area/lipid molecules ratio. Besides, PFD produces a decrease in the compressibility factor from 163 (for pure DSPA at π = 20 $mN.m^{-1}$) to 30 $mN.m^{-1}$ for the mixture DSPA:PFD 5:95 (Figure 4c) making the film more compressible. Based on this change in the compressibility factor, a transition from a condensed

View Article Online
DOI: 10.1039/C8SM02301H
Second Revision – SM-ART-11-2018-002301.R1

to an expanded state can be postulated for the film. The increase on the lift off area values at low pressures can be due to electrostatic repulsion between the negatively charged DSPA polar head groups and PFD molecules, which leads to a higher area per lipid molecule and to a more compressible monolayer. As the compression continues to smaller molecular areas and higher pressures are reached, the isotherms approach to the corresponding to pure DSPA for all PFD concentration values and no changes in mean molecular areas are observed (see Figure 4b, where $\Delta Mma = Mma_{with\ PFD} - Mma_{without\ PFD}$ vs $\%X_{PFD}$ at π = 40 mN.m^{-1} is plotted). This result is probably due to an expulsion and the further solubilization of PFD molecules at high pressure values. Also, as the molar fraction of PFD increases the compressibility factor decreases (Figure 4d) but the state of the film phase is not modified. Concerning to the collapse area and pressure, the presence of PFD does not induce significant changes (data not show).

Brewster angle images allow quantifying the reflectivity of the monolayer, following the gray level (GL) changes when a film of different refractive index with respect to water or lipidic film is present at the interface as well as determining the optical thickness of the film [43-44]. Figure 5 shows BAM images obtained for DSPA:PFD mixtures at molar fractions 100:0, 60:40 and 10:90 (corresponding to the isotherms in Figure 3a), and Figure 8a shows the corresponding GL for the different zones of the micrography: domains (circles) and continuous phase (squares). As it was previously discussed BAM images of pure DSPA, Figure 5a, show a condensed and homogeneous film in the whole range of pressure values studied. When the GL of the images are analyzed a gradual increase, until a constant value around 28, is observed. This increase is due to the organization of the hydrocarbon tail perpendicular to the air/water interface as compression takes places (Figure 8a, black squares). When PFD is present in the mixture at a low ratio (DSPA: PFD 60:40, Figure 5b) a different behavior is found with respect to pure DSPA. The first difference observed is the presence of non-homogeneous films at low pressures. At π = 3mN.m^{-1} light gray islets and dark domains, both immersed in a continuous phase, are observed (Figure 5b). The islets are, probably, zones of highly condensed pure lipid (gray level around 29, similar to that found for pure DSPA at high pressures) which becomes more homogeneous

View Article Online
DOI: 10.1039/C8SM02301H
Second Revision – SM-ART-11-2018-002301.R1

as pressure increases. On the other hand, the presence of dark domains (red circles on Figure 8a) with a gray level around 8, prevails until π = 20mN.m^{-1}, this structures are, probably, PFD enriched domains. Similar behavior was found for other perfluoroalkyl molecules and it was attributed to the lower reflective index of the fluorinated amphiphiles [45]. Dark domains disappear when surface pressure increases above π = 25mN.m^{-1}; at the same time Langmuir isotherm of the mixture approaches to that corresponding to pure DSPA, evidencing a PFD expulsion from the interface and further solubilization on water. This situation is probably induced by the electrostatic repulsion between PFD and DSPA, which becomes increasingly important as compression progresses, and also by the difference in the length of both hydrocarbon tails, which does not contribute to favorable van der Waals interactions. The hypothesis of PFD expulsion is also supported by the fact that the collapse area is still constant for all PFD fractions, Figure 3a, and the BAM images obtained above π = 25m.m^{-1} are homogeneous, condensed and with the same gray level than pure DSPA monolayer. All the evidence presented indicates that, at 60:40 molar ratio the DSPA:PFD mixture behaves as a non-miscible system at low surface pressure.

Figure 5c, shows BAM images for the mixture DSPA: PFD 10:90, in this case at low surface pressures the lipid is forming bright circular domains of DSPA/PFD (under these conditions the amount of PFD is high enough to avoid the formation of islets of pure DSPA), the gray level of the domains was lower than the corresponding to pure DSPA (blue square in Figure 8a), indicating a partial mixing with PFD. As the pressure increases the film becomes more homogeneous but with a gray level lower than pure DSPA and it presents dark elongate domains of PFD, similar to those found for DSPA:PFD 60:40. The continuous phase has a lower gray value than the corresponding to DSPA but they gradually resembles as pressure approaches to 25mN.m^{-1}, above this value the film is homogeneous and condensed (Figure 5c). These results can be interpreted as a partial mixing between DSPA and PFD at values π below 20mN.m^{-1}, above this value PFD is expelled from the interface.

View Article Online
DOI: 10.1039/C8SM02301H
Second Revision – SM-ART-11-2018-002301.R1

3.1.2. Effect of PFD on DSPE monolayers:

Figure 3b shows the Langmuir isotherms for DSPE and DSPE: PFD mixtures. DSPE exhibits an isotherm characterized for a collapse pressure and area around 55 $mN.m^{-1}$ and 38 $Å^2$, respectively, similar to values previously reported[46]. The compressibility modulus found at π = 40 $mN.m^{-1}$ is 265 $mN.m^{-1}$, which is within the characteristic values range for a condensed film. BAM images shows a homogeneous film at all the pressures studied (Figure 6a), with an average GL value of 32 (Figure 8b, black squares).

When PFD is present a similar effect to that obtained for the Langmuir isotherms of DSPA: PFD mixtures is found. The presence of PFD in hybrid DSPE:PFD monolayers is evident by the shift of the of the lift off areas to higher values (Figure 3d) and an increment in ΔMma at π = 20 $mN.m^{-1}$ (Figure 4a), more pronounced as PFD concentration increases. For higher π values, the Langmuir isotherms tend to resemble to that obtained for pure DSPE, indicating again a possible expulsion of PFD from the monolayer to the aqueous subphase. Also in this case, increasing PFD molar fraction leads to a decrease in the Cs^{-1} modulus, more evident at low pressure values: from 200 to 50 $mN.m^{-1}$ at π = 20 $mN.m^{-1}$ and from 270 to 150 $mN.m^{-1}$ at π = 40$mN.m^{-1}$ (Figure 4c-d). It can be concluded that the presence of PDF in the mixtures produces an increment in the film compressibility. Concerning to BAM images (Figure 6b) the presence of PFD in the DSPE:PFD 60:40 mixture induces the segregation of a PFD enriched phase with lower GL value than the corresponding to pure DSPE at π > 20 $mN.m^{-1}$, the appearance is of dark elongated domains[45], with a GL value between 10-20 (Figure 8b). When surface pressure increases the second phase disappears and the average GL value resembles to that corresponding to pure DSPE, probably due to an expulsion of PDF from the interface.

For DSPE:PFD 10:90 mixture, a different behavior was found (Figure 6c): under this condition the dark elongate domains are not formed at any pressure, on the contrary the formation of a continuous phase with a GL value lower than the corresponding to DSPE is evident at all pressures (Figure 8b).

View Article Online
DOI: 10.1039/C8SM02301H
Second Revision – SM-ART-11-2018-002301.R1

Moreover, from Figure 6c it can be observed the presence of zones with average GL = 64, higher than that for DSPE ($GL_{maximunm}$ = 34) which persist at all pressures. At this molar fraction it is probably that the miscibility between DSPE and PFD increases giving rise to a phase with an intermediate gray value, formed by the mixture of both component, along with the formation of pure DSPE aggregates (higher gray level than DSPE).

3.1.3. Effect of PFD on DLPA monolayers:

Figure 3c shows the Langmuir isotherms for pure DLPA and DLPA:PFD mixtures. DLPA isotherm shows a phase transition from liquid expanded to liquid condensed phase around π = 31 $mN.m^{-1}$. At the present experimental conditions, the value of Cs^{-1} factor at the liquid expanded (π = 20 $mN.m^{-1}$) and liquid condensed (π = 40 $mN.m^{-1}$) phases are 56 $mN.m^{-1}$ and 165 $mN.m^{-1}$, respectively. The collapse area and pressure are 38 $Å^2$ and 57 $mN.m^{-1}$ respectively. Figure 7a shows BAM images for DLPA in the absence of PFD. As it can be seen the images for the liquid expanded monolayer, at surface pressures below 30$mN.m^{-1}$, indicate a homogeneous phase, with a maximum GL value of 4 (Figure 8c, black squares). From π = 30$mN.m^{-1}$, the appearance of liquid - condensed nucleus (seeds) and the growth of domains around these seeds can be noted. These domains lead to a homogeneous condensed phase at high pressure values, with an average GL of 9 (Figure 8c-black circles).

The increment in PFD molar fraction induces an increase in mean molecular area (Figure 4a) and in lift off area (Figure 3d), together with a decrease in Cs^{-1} (Figure 4c and d), leading to a more compressible monolayer. The increase in mean molecular area is more important at low pressure values, but this effect is preserved at surface pressure values above the phase transition (Figure 4 a and b) and, as can be noted in the Langmuir isotherms, the collapse mean molecular area in the presence of PFD is higher than the corresponding to pure DLPA monolayer, probably due to the persistence of PFD molecules at the interface even at high surface pressures.

View Article Online
DOI: 10.1039/C8SM02301H
Second Revision – SM-ART-11-2018-002301.R1

BAM images obtained in the presence of PFD, under the same conditions than isotherms in Figure 3c, are shown in Figures 7 b-c, while the GL values determined from these images are plotted in Figure 8 c as a function of π. As can be seen in Figure 7 b-c the hybrid DLPA:PFD films form a homogeneous monolayer below π = 20 mN.m^{-1} and 10 mN.m^{-1} for the ratios DLPA:PFD 60:40 and 10:90, respectively. Above these pressures the appearance of the nucleation centers for the condensed phase is evident and the pressure values from which this centers start to appear are gradually smaller as PFD molar fraction increases (Figures 7 b-c) Figure 9 shows the images of monolayers formed by mixtures DLPA: PFD, at ratios 100:0, 60:40 y 10:90, obtained at the 60% of phase transition in all cases, i.e. 60 % of the whole films correspond to the condensed phase. The condition of 60 % of phase transition was reached at the following surface pressure values:

Ratio DLPA: PFD:	100:0	60:40	10:90
Surface pressure:	31 mN.m^{-1}	30,7 mN.m^{-1}	30 mN.m^{-1}

From these images, the domains numbers and areas can be calculated for the same phase transition state. Then, when surface pressure increases the growing of domains occurs, and, as can be seen in Figure 9 a, the presence of PFD induces the formation of a higher number of domains with a lower area. Figure 9 b shows the number and average area of domains obtained from images on Figure 9 a. The number of domains increases from 9 in absence of PFD to 39 for PFD ratio 90% (red circles), and the corresponding average areas change from 681 μm^2 to 145 μm^2, respectably (pink bars). At this point, we can postulate that PFD prevents lipid diffusion and, for this reason, the formation of a new domains in the presence of PFD is more favorable than the growth of a pre-existing one [44]. Previous works demonstrate that perfluoroalkyl molecules can be used for modulate the topography of lipid membranes[30].

Concerning to the quantification of the gray level from BAM images (Figure 8 c), the mixture DLPA:PFD presents two zones of gray level, similar to the results for pure DLPA, the first corresponds

View Article Online
DOI: 10.1039/C8SM02301H
Second Revision – SM-ART-11-2018-002301.R1

to the liquid expanded phase (squares in Figure 8 c) and the second one is related to the condensed phase (circles in Figure 8 c). When PFD was present in a 40% molar fraction no changes were detected on gray level with respect to pure DLPA monolayer, but if the molar fraction of PFD increases up 90 % a markedly decrease on gray level for both phases was detected. This decrease in gray level was around of 50% for both phases and it matched with a decrease in the contrast between liquid expanded and condensed phases. This effect together with the increase in domain number and the linear decrease in the pressure of apparition of domains, support the hypothesis of a miscible mixture between DLPA and PFD under this concentration and surface pressure conditions[33]. For DLPA:PFD mixtures segregation of PFD was not found, probably for a higher affinity between them, due to a similar hydrocarbon length (DLPA: 12 carbon atoms and PFD: 10 carbon atoms).

3.2. Insertion of PFD in pre-formed monolayer and exclusion pressure determination

PFD penetration into monolayers of DSPA, DSPE and DLPA was characterized through adsorption isotherms and experiments based on constant surface-area approach, using $1x10^{-2}$ M LiCl as the subphase. With the aim of determining the concentration at which the monolayers were saturated by PFD molecules, the phospholipids monolayers were pre-formed at a constant pressure and the effect of increasing PFD concentration on surface pressure was studied, Figure 10 a (where $\Delta\pi_i = \pi_{t=30min} - \pi_{t=0}$ is the pressure change recorded after 30 min elapsed from injection at the subphase of each PFD concentration with respect to the pressure before the injection). PFD concentration at which the surfactant adsorption reaches the maximum value, with no further changes in the surface pressure with subsequent increase in PFD concentration, was determined. This value corresponds to the saturation concentration (SC), and it was used for the determination of exclusion pressure. The SC values obtained were 0.52 mM, 1.6 m M and 1.7 mM, for DSPE, DLPA and DSPA respectively, Table 1. The curves of $\Delta\pi_i$ vs PFD concentration can be adjusted with a hyperbolic function and the maximum change in surface pressure generated by PFD ($\Delta\pi_{max}$) can be determined as well as the K0.5 parameter. K0.5

View Article Online
DOI: 10.1039/C8SM02301H
Second Revision – SM-ART-11-2018-002301.R1

reflects the ability of PFD to induce a change in molecular packing of the monolayer. The plots of $\Delta\pi_i$ vs PFD concentration were transformed to the reciprocal 1/ $\Delta\pi_i$ vs 1/ C_{PFD}, inset in Figure 10 a, and from the linear regression $\Delta\pi_{max}$ and K0.5 can be obtained from[47]:

$$\frac{1}{\Delta\pi} = \frac{1}{\Delta\pi_{max}} + \frac{K0.5}{\Delta\pi_{max}} x \frac{1}{C_{PFD}}$$

The values of $\Delta\pi_{max}$ and K0.5 obtained are shown in table 1. As can be seen, the $\Delta\pi_{max}$ values obtained (18 mN.m^{-1} for DSPA, 29 mN.m^{-1} for DSPE and 33 mN.m^{-1} for DLPA) are demonstrating that PDF induce the following decreasing order in pressure change: DLPA > DSPE>DSPA. A different tendency was found for K0.5 values. DSPA and DLPA have almost the same value, around 0.5 mM, effect that can be understood taking into account that both lipids have the same polar head and charge, so the ability of PFD to induce changes in the molecular package when it access to the monolayer from the subphase was the same. On other hand, PFD has the highest effect on the molecular package of DSPE, which corresponds to the lowest value of K0.5 (0.2 mM), this result can be interpreted taking into account the zero net charge of DSPE at the interface, unlike the negative polar head groups of DSPA and DLPA. In this way, PFD (negatively charged) exhibits less electrostatic repulsion with DSPE monolayer, producing a higher disturbing effect.

Once SC was determined for each lipid, the determinations of exclusion pressures were carried out. For this purpose, experiments at different initial surface pressures were performed and the change in surface pressure produced by the addition of PFD, at the corresponding SC, in the subphase was recorded and plotted as a function of the initial pressure, Figure 10 b (as described above in section 2.2.2 and figure 2). The exclusion pressure value indicates the surface pressure above which PFD does not penetrate the lipid monolayer [48-50], the resulting values are summarized in table 1. In the case of DLPA this value was calculated taking into account only the condensed phase, with the aim of comparing the effect of PFD at the same phase state (liquid condensed) for all systems. The values obtained for exclusion pressure were 34 mN.m^{-1}, 41 mN.m^{-1} and 44 mN.m^{-1}, for DSPA, DSPE and DLPA respectably. These values indicate that PDF can penetrate at higher pressure values in the DLPA

View Article Online
DOI: 10.1039/C8SM02301H
Second Revision – SM-ART-11-2018-002301.R1

monolayer, followed by DSPE and DSPA. It is important to remark that all values of exclusion pressure are higher than the proposed surface pressure for lipid bilayer of 30 $mN.m^{-1}$ [51], and this fact probably indicates than PFD can remain in lipid bilayers once it penetrates them. Exclusion pressure values can be interpreted as a measure of the stability of the PFD-Lipid mixture, and, in this sense, the mixture with DLPA should be the most stable one, also demonstrated by previous experiments.

3.3. Effect of PFD on LUVs.

With the aim of evaluating the detergent effect of PFD, LUVs of DSPA and DLPA were synthesized and exposed to increasing concentrations of PFD. These experiments were followed by nephelometry and dynamic light scattered. At this point it is important to remark that DSPE does not form LUVs under the present experimental conditions, LiCl $1x10^{-2}$ M.

Figure 11 a shows the percentage of relative turbidity as a function of PFD concentration for DLPA (red) and DSPA (black) vesicles, and Figures 11 b and 11 c show the evolution of hydrodynamic size of LUVs with PFD concentration at the points remarked in Figure 11 a (points 1, 2 and 3). In general, the relative turbidity decrease corresponds to LUVs breaking off [52-53]. In the case of DSPA, LUVs have an average diameter of (71±13) nm in the absence of PFD, point (1) in Figures 11 a and c. After increasing PFD concentration to 20 μM (point (2) in Figures 11 a and c), the vesicles size increases up to a value of (126±20) nm, probably due to the insertion of PFD molecules into the DSPA vesicles, hypothesis supported by exclusion pressure values. In parallel, a percentage of vesicles break off in accordance with a decrease in %RT, and an average size of (27±7) nm. A subsequent increase in PFD concentration induces the breaking off of all DSPA LUVs, point (3) Figure 11 a and c, under these conditions the average size obtained is (1.0±0.2) nm, in accordance with the constant low value of %RT. Partial solubilization produced by perfluoroalkyl molecules were found for DSPC and DPPC vesicles[34].

View Article Online
DOI: 10.1039/C8SM02301H
Second Revision – SM-ART-11-2018-002301.R1

The effect of PFD on DLPA LUVs is different to that found for DSPA. In the absence of PFD, DLPA LUVs have an average size of (84±16) nm. When PDF is added to a final concentration of 18 μM, Figure 11 a and b point 2, a fraction of vesicles breaks off and gives origin to a population with an average diameter of (24±4) nm, effect in agreement with a decrease in %RT. At the same time, a second population of LUVs with a similar diameter to bare DLPA vesicles is present, (87±17) nm. A subsequent increase in PFD concentration to 62 μM, Figure 11 a and c point 3, induces an enhance in the LUVs fraction with smaller diameters but bigger than those corresponding to point 2, (56±9) nm; and the population with higher sizes increases their diameter to (147±24) nm. For both populations the increase in size is in agreement with the exclusion pressure values obtained: PFD can penetrate the monolayer of DLPA until a pressure of 44 $mN.m^{-1}$, which is higher than the value accepted for surface pressure of a lipidic bilayer. In this case the decrease in %RT remains still constant at a value of almost 50% for the higher PFD concentration analyzed, effect probably due to non-completely disruption of the vesicles, as a consequence of the miscibility between DLPA and PFD, and the formation of a hybrid vesicle. Similar swelling behavior of vesicles produced by perfluoroalkyl molecules were found for DMPC[34].

4. Discussion

In the present work the lipid molecules were chosen taken into account the charge of the polar head, negative (PA) and zwiterionic (PE), to evaluate the effect of electrostatic interactions between them and PFD, as well as the length of the hydrocarbon tail, C18 (DS) and C12 (DL) to evaluate the hydrophobic interactions between the lipids and PFD. As can be seen in Figure 3, PFD does not exhibit

View Article Online
DOI: 10.1039/C8SM02301H
Second Revision – SM-ART-11-2018-002301.R1

a stable Langmuir isotherm and, for this reason, Langmuir isotherm of lipid:PFD mixtures were plotted as a function of the mean molecular area of the phospholipids.

When the Langmuir monolayers were generated in the presence of PFD a general increase in mean molecular areas of the lipids at low surface pressure values was found for all the lipid studied. This effect was more evident for DLPA with respect to DSPA and DSPE. The increase in area for DLPA caused by PFD at a concentration ratio of 90% and at π = 20 mN.m^{-1}, Figure 4, was 40Å^2 while for DSPE and DSPA it was 15 Å^2, the difference can be explained taking into account the state of phase of the monolayer, in the case of DLPA the monolayer was in liquid expanded phase while DSPE and DSPA were in a liquid condensed phase. When the pressure was increased to π = 40 mN.m^{-1}, DLPA was in condensed phase, the change in area caused by PFD decreased to 10 Å^2 close to the values obtained for DSPA and DSPE in the same phase state. Then, an important conclusion arises: PFD produces a higher expansive effect on the monolayer in an expanded phase compared to those in a condensed state. The expansion of the monolayers was accompanied with a decrease in the compressibility factor, so that the monolayers were more compressible in the presence of PFD with respect to in the absence of PFD, for all the lipids analyzed. Other important observation is related with the fact that at high pressure values PFD was expelled from the interface in the case of DSPE and DSPA monolayers, the pressure and area of collapse did not change when increasing the fraction of PFD.

When BAM images of lipid:PFD mixtures were analyzed different features were found depending of the lipid analyzed. In the case of DSPA, at low surface pressure values, the presence of PFD was evident by the formation of dark domains which disappeared at high surface pressure values. For DSPA:PFD mixtures the gray level of the continuous phase was always the same at low PFD molar fractions, Figure 5 and 8 a-squares. DSPA is a phospholipid with 18 carbon atoms in its backbone and PFD has 10 carbon atoms in its fluorinated chain, so that, there is a difference of 1.232 nm in the length of their hydrophobic chains (assuming a C-C bond distance equal to 154 pm for the eight C-C bond), this difference can generate an ¨hydrophobic mismatch¨[54], situation energetically unfavorable for PFD

View Article Online
DOI: 10.1039/C8SM02301H
Second Revision – SM-ART-11-2018-002301.R1

and DSPA interaction at the air/water interface. So, the system stabilizes itself segregating PFD to diminish the boundary energy between PFD and DSPA, and at a certain value of surface pressure for which the monolayer is more oriented, above 20mN.m^{-1} for the ratio 60:40, PFD is expelled from the interface and the domains disappear. For DSPA monolayer, the miscibility behavior depends on the molar fraction of PFD: at lower values the system has non-miscible behavior at all surface pressures. The gray level, in this case, was the same than that for pure DSPA and PFD molecules were segregated in domains to be further expelled at higher pressures. At higher PFD fractions the mixture behaves like a partially miscible one, but when the system reaches certain surface pressure values, PFD molecules are expelled from the interface. An opposite behavior was observed for the mixture DLPA:PFD, in this case BAM images did not show the presence of dark domains and the gray level of the continue phase was always lower than the corresponding to pure lipid. This evidence, in combination with the decrease in size and increase in number of condensed domain in LE/LC transition, were evidences of miscibility between both components. The difference between DLPA and PFD length is 0.154nm (one C-C bond) and, in this case, the energetic cost of segregating PFD is higher than mixing energy between them. Dupuy and Maggio, found a similar effect between mixed monolayers of ceramides, the mixture between Cer10:Cer12 led to a completely miscible system at all surface pressures and molar fractions, on the contrary the mixture Cer10:Cer18 led to an immiscible behavior under all conditions [55], effect due to the difference in mismatch found between the two mixtures: for Cer10:Cer12 there is a mismatch of 2 C atoms (equivalent to PFD:DLPA) while for Cer10:Cer18 there is a mismatch of 8 C (equivalent to PFD:DSPA). The case of DSPE:PFD can be considered as an intermediate system, when the molar fraction of PFD was lower than 50%, the system behaves like PFD:DSPA (60:40), in this case the system segregates PFD to diminish the energetic cost of the mismatching, BAM images showed elongate dark domains (Figure 6 and 8 b) and the continuous phase has the same gray level than DSPE monolayer, Figure 8 b-squares. Nevertheless, when PFD fraction was increased to 90% the system partially mixes producing a decrease in gray level in BAM images at all pressure values, at this point the process is probably more favorable due to the energy gained by interaction between the polar head

View Article Online
DOI: 10.1039/C8SM02301H
Second Revision – SM-ART-11-2018-002301.R1

groups of DSPE and PFD (electrostatic interaction) compensating the energetic cost of maintaining the mismatch. Also, the presence of bright domains of DSPE aggregates was observed in BAM images, at this point DSPE was segregated.

Adsorption isotherms of PFD over preformed monolayers of DSPA, DLPA and DSPE were also carried out. From these experiments the values of $\Delta\pi_{max}$ and K0.5 were calculated by fitting the curves with a model that assume the existence of finite number of binding sites, without restriction of different types of interaction sites [47]. The values obtained from this fitting are shown in table 1.

The tendency found in $\Delta\pi_{max}$ for negative lipids, DLPA >DSPA can be explained taken into count the compressibility of DLPA and DSPA monolayer. Both lipids have the same net charge but DLPA monolayer is more expanded and compressible than DSPA monolayer, so PFD can penetrate and induce a higher change at the same concentration. On the other hand, DSPE showed an intermediate behavior, probably because the effect of PFD on DSPE monolayer was driven by two opposing factors: (1) the zero net charge, which favors the insertion and (2) a condensed and less compressible film which prevents the insertion. From K0.5 values informed in table 1, it can be seen that the modification of the monolayer packaging depends on the electrostatic repulsion between PFD and the lipid molecule, independent on the film compactness which was confirmed since the K0.5 values for DSPA and DLPA were the same, 0.5 mM. Instead, an important effect of the interfacial charge can be postulated, confirmed by the fact that the K0.5 value for PFD penetration on DSPE (zwiterionic) monolayer was a half (0.2mM) of the values found for the negative lipids. PFD can disturb the monolayer of DSPE more efficiently because non electrostatic repulsions are limiting the adsorption.

On other hand, exclusion pressure values (Figure 10) showed that PFD can penetrate the monolayers until: 44 $mN.m^{-1}$ for DLPA, 41 $mN.m^{-1}$ for DSPE and 34 $mN.m^{-1}$ for DSPA. When compared the same polar head of lipid but with different hydrocarbon tail, PFD could penetrate until higher pressure values in an expanded monolayer as DLPA. But, when the charge of the polar head group of the lipid was studied for the same hydrocarbon tail, PFD penetrated at higher pressure values in DSPE monolayer compared to DSPA films. The higher insertion into the DSPE monolayer was due to the

View Article Online
DOI: 10.1039/C8SM02301H
Second Revision – SM-ART-11-2018-002301.R1

zwiterionic nature of the monolayer, as PFD molecules are negatively charged there is a higher electrostatic repulsion between them and DSPA compared to DSPE. Similar effects were found for the insertion of E1 peptide on monolayers of DMPC, DMPG and POPG[56]. The most interesting point found from these experiments is the fact that PFD can penetrate the Langmuir monolayer up pressure values higher than those reported for a cellular bilayer, independently of the lipid nature and could cause several problems considering PFD as a potentially toxic compound for cells. Due to the structural similarity between PFD and the lipid molecules, these surfactants can mimic with membrane and alter its functions.

For a better understanding of PFD effect over a model of lipidic bilayer, large unilamelar vesicles (LUVs) of DLPA and DSPA were synthetized and exposed to increasing concentrations of PFD. The evolution of the experiments was followed by nephelometry and dynamic light scattering (DLS). The results indicate that PFD has a lytic effect over DSPA LUVs above a PFD concentration of 40 μM, but below this concentration value, PFD aggregates produce an increase in the diameter. This can be explained taking in to account the values of exclusion pressure obtained under these conditions which indicate that PFD can adsorb into the monolayer up π = 34 mN.m^{-1}. A possible explanation for the initial increase in size and the later rupture can be a similar effect to that found for monolayers, at a certain pressure value the vesicle becomes unstable, due to the mismatch difference between the two molecules. In the case of DLPA, PFD induces a partial lysis of a fraction of vesicle at 18 μM and the population of (87±17) nm remains unaltered. Further increase of PFD concentration, 62 μM, generates a size increase of both populations of LUVs. In the same way than the case of DSPA, PFD penetrate DLPA LUVs increasing their size. Unlike the case of DSPA, PFD can adsorb on DLPA up to higher surface pressures values (exclusion pressure value: 44 mN.m^{-1}). PFD does not have a lytic effect within the range of concentrations analyzed and DLPA:PFD form a stable mixture at the interface due to the small mismatch difference.

5. Conclusions

View Article Online
DOI: 10.1039/C8SM02301H
Second Revision – SM-ART-11-2018-002301.R1

With the aim to characterize the mixing properties of PFD with membranes models several experiments were systematically carried out for DSPA, DSPE and DLPA lipidic monolayers. The present lipids were selected in such way to allow evaluating the influence of the lipid charge and the phase state (molecular compactness) on the miscibility with PFD molecules.

Taking into account the systems studied it is important to analyze three factors for understanding the global effect of PFD over lipid membranes:

- Electrostatic repulsion between polar head groups.
- Molecular packing of the monolayer.
- Mismatching differences between PFD and the lipid under study.

From Langmuir isotherms of Lipid:PFD mixtures it was evident that PFD increased the occupied area per lipid and the magnitude of the change depends on the film compactness, supported by the fact that the most affected lipid was DLPA. This expansive effect was accompanied with a decrease in compressibility factor (monolayer makes more compressible), more evident at lower pressure values. BAM images demonstrated that DSPA:PFD and DSPE:PFD monolayers at high PFD molar fractions segregate PFD in dark domains of a lower gray level at low surface pressure values, making evident a non-miscible system. A further increase in lateral pressure produces the expulsion of PFD from the interface. This result was explained taking into account the compactness of DSPA and DSPE films and the mismatching between PFD and these lipids. In the case of DSPE at high PFD molar fractions and DLPA at all PFD molar fractions, the system does not segregate PFD, on the contrary a completely miscible films were observed by BAM, with a decrease in gray level at all lateral pressure values. For DSPE the change of the behavior with PFD concentration can be understood considering favorable interactions between polar head of DSPE and PFD (hydrogen bonding). In the case of DLPA:PFD mixtures the mismatching between them was of one C-C bond witch not implies an extra energetic cost, so that DLPA stabilizes PFD on the interface through hydrophobic interactions and form a miscible system. Other evidence of miscibility between DLPA and PFD, is the fact that PFD affect the domains

View Article Online
DOI: 10.1039/C8SM02301H
Second Revision – SM-ART-11-2018-002301.R1

nucleation of the liquid expanded/liquid condensed transition of DLPA, PFD acts like an hindrance for lipid diffusion and the obtained domains were smaller and in greater quantity as the concentration of PFD increases. At this point we can conclude that a mixture lipid:PFD behaves as a miscible or as a not-miscible system depending on the interactions between the components and of the mismatching between them.

Concerning to the adsorption experiments the value of K0.5 obtained reveals that the ability to induce changes in molecular packing depends on electrostatic affinity between PFD and Lipid, the values found for PFD penetration does not distinguish the hydrocarbon tails but depends on the net charge of the polar head group, demonstrating more affinity for neutral lipid than for the negative ones. On other hand, the maximum pressure obtained from adsorption isotherms was highly dependent on the film compactness, given the highest value for DLPA (more expanded monolayer) and the lowest value for DSPA (more compact monolayer).

One of the more interesting result obtained, was the fact that PFD incorporate at surface pressure values higher than 25 – 30 $mN.m^{-1}$ on the monolayers, specifically at 34 $mN.m^{-1}$, 41 $mN.m^{-1}$ and 44 mNm^{-1} for DSPA, DSPE and DLPA, respectively. As can be seen, the biggest value found corresponds to DLPA monolayer and the smallest to DSPA. Indeed, DLPA has a better structural similarity with PFD and its monolayer is more expanded than DSPA. Moreover, exclusion pressure value of DSPE is higher than that for DSPA, due to the absence of electrostatic repulsion when it is inserted.

When the effect of PFD was studied on vesicles we found that PFD inserts on DSPA and DLPA LUVs, effect checked by an increase in the average size. But in the case of DSPA an enhance in PFD concentration induce a lytic effect, and all LUVs population broke off. In the case of DLPA vesicles increase in size forming a hybrid bilayer, in concordance with exclusion pressure values and monolayer studies, the mixtures DLPA/PFD were more stable.

With all the evidences described above we can propose a model for the two extreme cases, Figure 12:

View Article Online
DOI: 10.1039/C8SM02301H
Second Revision – SM-ART-11-2018-002301.R1

(A) DSPA:PFD mixtures are immiscible at high molar fraction of PFD.

(B) DLPA:PFD and DSPE:PFD mixtures are miscible at low molar fraction.

Finally, our findings suggest than PFD could have negative effects on biological and environmental systems. PFD can penetrate and adsorb on membranes models (LUVs or monolayers) at similar surface pressure values than those proposed for the lateral pressure in a cellular bilayer independently on the lipid composition (condensed or expanded film, neutral o charged). This fact can have several effects, modifying the bilayer from a structural point and altering its functionality. These molecules are a kind of contaminants present in the environment that are acquired a lot of relevance in the last few years.

Acknowledgments

This work was supported by SECyT-UNC, CONICET and FONCYT. L. M. Yudi and C. I. Camara are Career Investigators and Viada. B is a scholar fellow of CONICET. The BAM measures were done on the Centro de Microscopía Optica y Confocal de Avanzada de Córdoba (CEMICO), integrated to the Sistema Nacional de Microscopía (SNM-MINCyT).

View Article Online
DOI: 10.1039/C8SM02301H
Second Revision – SM-ART-11-2018-002301.R1

References:

1. Buck, R. C.; Franklin, J.; Berger, U.; Conder, J. M.; Cousins, I. T.; de Voogt, P.; Jensen, A. A.; Kannan, K.; Mabury, S. A.; van Leeuwen, S. P. J., Perfluoroalkyl and Polyfluoroalkyl Substances in the Environment: Terminology, Classification, and Origins. *Integrated Environmental Assessment and Management* **2011,** *7* (4), 513-541.

2. Viberg, H.; Eriksson, P., Chapter 47 - Perfluorooctane sulfonate (PFOS) and perfluorooctanoic acid (PFOA). In *Reproductive and Developmental Toxicology*, Gupta, R. C., Ed. Academic Press: San Diego, 2011; pp 623-635.

3. Butenhoff, J. L.; Pieterman, E.; Ehresman, D. J.; Gorman, G. S.; Olsen, G. W.; Chang, S.-C.; Princen, H. M. G., Distribution of perfluorooctanesulfonate and perfluorooctanoate into human plasma lipoprotein fractions. *Toxicology Letters* **2012,** *210* (3), 360-365.

4. Zhang, Y.; Beesoon, S.; Zhu, L.; Martin, J. W., Biomonitoring of Perfluoroalkyl Acids in Human Urine and Estimates of Biological Half-Life. *Environmental Science & Technology* **2013,** *47* (18), 10619-10627.

5. Chen, H.; Zhang, C.; Han, J.; Yu, Y.; Zhang, P., PFOS and PFOA in influents, effluents, and biosolids of Chinese wastewater treatment plants and effluent-receiving marine environments. *Environmental Pollution* **2012,** *170*, 26-31.

6. Bossi, R.; Riget, F. F.; Dietz, R.; Sonne, C.; Fauser, P.; Dam, M.; Vorkamp, K., Preliminary screening of perfluorooctane sulfonate (PFOS) and other fluorochemicals in fish, birds and marine mammals from Greenland and the Faroe Islands. *Environmental Pollution* **2005,** *136* (2), 323-329.

7. Yeung, L. W. Y.; De Silva, A. O.; Loi, E. I. H.; Marvin, C. H.; Taniyasu, S.; Yamashita, N.; Mabury, S. A.; Muir, D. C. G.; Lam, P. K. S., Perfluoroalkyl substances and extractable organic fluorine in surface sediments and cores from Lake Ontario. *Environment International* **2013,** *59*, 389-397.

View Article Online
DOI: 10.1039/C8SM02301H
Second Revision – SM-ART-11-2018-002301.R1

8. Hopkins, Z. R.; Sun, M.; DeWitt, J. C.; Knappe, D. R. U., Recently Detected Drinking Water Contaminants: GenX and Other Per- and Polyfluoroalkyl Ether Acids. *Journal - American Water Works Association* **2018,** *110* (7), 13-28.

9. Guelfo, J. L.; Adamson, D. T., Evaluation of a national data set for insights into sources, composition, and concentrations of per- and polyfluoroalkyl substances (PFASs) in U.S. drinking water. *Environmental Pollution* **2018,** *236*, 505-513.

10. Hu, X. C.; Andrews, D. Q.; Lindstrom, A. B.; Bruton, T. A.; Schaider, L. A.; Grandjean, P.; Lohmann, R.; Carignan, C. C.; Blum, A.; Balan, S. A.; Higgins, C. P.; Sunderland, E. M., Detection of Poly- and Perfluoroalkyl Substances (PFASs) in U.S. Drinking Water Linked to Industrial Sites, Military Fire Training Areas, and Wastewater Treatment Plants. *Environmental Science & Technology Letters* **2016,** *3* (10), 344-350.

11. Suuberg, J. L. G. T. M. D. M. K. D. A. S. S. F. M. C. E. M., Evaluation and Management Strategies for Per- and Polyfluoroalkyl Substances (PFASs) in Drinking Water Aquifers: Perspectives from Impacted U.S. Northeast Communities. *Environ Health Perspect* **2018,** *126* (6), 065001-1 to 065001-13.

12. Kannan, K.; Corsolini, S.; Falandysz, J.; Fillmann, G.; Kumar, K. S.; Loganathan, B. G.; Mohd, M. A.; Olivero, J.; Wouwe, N. V.; Yang, J. H.; Aldous, K. M., Perfluorooctanesulfonate and Related Fluorochemicals in Human Blood from Several Countries. *Environmental Science & Technology* **2004,** *38* (17), 4489-4495.

13. Olsen, G. W.; Mair, D. C.; Lange, C. C.; Harrington, L. M.; Church, T. R.; Goldberg, C. L.; Herron, R. M.; Hanna, H.; Nobiletti, J. B.; Rios, J. A.; Reagen, W. K.; Ley, C. A., Per- and polyfluoroalkyl substances (PFAS) in American Red Cross adult blood donors, 2000–2015. *Environmental Research* **2017,** *157*, 87-95.

14. Moriwaki, H.; Takata, Y.; Arakawa, R., Concentrations of perfluorooctane sulfonate (PFOS) and perfluorooctanoic acid (PFOA) in vacuum cleaner dust collected in Japanese homes. *Journal of Environmental Monitoring* **2003,** *5* (5), 753-757.

View Article Online
DOI: 10.1039/C8SM02301H
Second Revision – SM-ART-11-2018-002301.R1

15. Sanchez Garcia, D.; Sjödin, M.; Hellstrandh, M.; Norinder, U.; Nikiforova, V.; Lindberg, J.; Wincent, E.; Bergman, Å.; Cotgreave, I.; Munic Kos, V., Cellular accumulation and lipid binding of perfluorinated alkylated substances (PFASs) – A comparison with lysosomotropic drugs. *Chemico-Biological Interactions* **2018,** *281*, 1-10.

16. Rainieri, S.; Conlledo, N.; Langerholc, T.; Madorran, E.; Sala, M.; Barranco, A., Toxic effects of perfluorinated compounds at human cellular level and on a model vertebrate. *Food and Chemical Toxicology* **2017,** *104*, 14-25.

17. Rockwell, C. E.; Turley, A. E.; Cheng, X.; Fields, P. E.; Klaassen, C. D., Persistent alterations in immune cell populations and function from a single dose of perfluorononanoic acid (PFNA) in C57Bl/6 mice. *Food and Chemical Toxicology* **2017,** *100*, 24-33.

18. Lau, C.; Thibodeaux, J. R.; Hanson, R. G.; Narotsky, M. G.; Rogers, J. M.; Lindstrom, A. B.; Strynar, M. J., Effects of Perfluorooctanoic Acid Exposure during Pregnancy in the Mouse. *Toxicological Sciences* **2006,** *90* (2), 510-518.

19. Rainieri, S.; Conlledo, N.; Larsen, B. K.; Granby, K.; Barranco, A., Combined effects of microplastics and chemical contaminants on the organ toxicity of zebrafish (Danio rerio). *Environmental Research* **2018,** *162*, 135-143.

20. Tang, J.; Jia, X.; Gao, N.; Wu, Y.; Liu, Z.; Lu, X.; Du, Q.; He, J.; Li, N.; Chen, B.; Jiang, J.; Liu, W.; Ding, Y.; Zhu, W.; Zhang, H., Role of the Nrf2-ARE pathway in perfluorooctanoic acid (PFOA)-induced hepatotoxicity in Rana nigromaculata. *Environmental Pollution* **2018,** *238*, 1035-1043.

21. Song, X.; Tang, S.; Zhu, H.; Chen, Z.; Zang, Z.; Zhang, Y.; Niu, X.; Wang, X.; Yin, H.; Zeng, F.; He, C., Biomonitoring PFAAs in blood and semen samples: Investigation of a potential link between PFAAs exposure and semen mobility in China. *Environment International* **2018,** *113*, 50-54.

22. Steves, A. N.; Turry, A.; Gill, B.; Clarkson-Townsend, D.; Bradner, J. M.; Bachli, I.; Caudle, W. M.; Miller, G. W.; Chan, A. W. S.; Easley, C. A. I., Per- and polyfluoroalkyl substances impact human spermatogenesis in a stem-cell-derived model. *Systems Biology in Reproductive Medicine* **2018,** *64* (4), 225-239.

View Article Online
DOI: 10.1039/C8SM02301H
Second Revision – SM-ART-11-2018-002301.R1

23. VanNoy, B. N.; Lam, J.; Zota, A. R., Breastfeeding as a Predictor of Serum Concentrations of Per- and Polyfluorinated Alkyl Substances in Reproductive-Aged Women and Young Children: A Rapid Systematic Review. *Current Environmental Health Reports* **2018,** *5* (2), 213-224.

24. Melzer, D.; Rice, N.; Depledge, M. H.; Henley, W. E.; Galloway, T. S., Association between Serum Perfluorooctanoic Acid (PFOA) and Thyroid Disease in the U.S. National Health and Nutrition Examination Survey. *Environmental Health Perspectives* **2010,** *118* (5), 686-692.

25. Broniatowski, M.; Sandez Macho, I.; Dynarowicz-Łątka, P., Study of perfluorooctyl-n-alkanes monolayers at the air–water interface. *Thin Solid Films* **2005,** *493* (1), 249-257.

26. Broniatowski, M.; Vila Romeu, N.; Dynarowicz-Łątka, P., Study of the collapse mechanism of selected fluorinated surfactants. *Journal of Colloid and Interface Science* **2008,** *325* (2), 464-471.

27. Nakahara, H.; Nakamura, S.; Kawasaki, H.; Shibata, O., Properties of two-component Langmuir monolayer of single chain perfluorinated carboxylic acids with dipalmitoylphosphatidylcholine (DPPC). *Colloids and Surfaces B: Biointerfaces* **2005,** *41* (4), 285-298.

28. Xie, W.; Kania-Korwel, I.; Bummer, P. M.; Lehmler, H. J., Effect of potassium perfluorooctanesulfonate, perfluorooctanoate and octanesulfonate on the phase transition of dipalmitoylphosphatidylcholine (DPPC) bilayers. *Biochimica et Biophysica Acta (BBA) - Biomembranes* **2007,** *1768* (5), 1299-1308.

29. Yokoyama, H.; Nakahara, H.; Shibata, O., Miscibility and phase behavior of DPPG and perfluorocarboxylic acids at the air–water interface. *Chemistry and Physics of Lipids* **2009,** *161* (2), 103-114.

30. Paige, M. F.; Eftaiha, A. a. F., Phase-separated surfactant monolayers: Exploiting immiscibility of fluorocarbons and hydrocarbons to pattern interfaces. *Advances in Colloid and Interface Science* **2017,** *248*, 129-146.

31. Saito, H.; Shinoda, W.; Mikami, M., Fluorination effects on structure and dynamics of phospholipid bilayer: A molecular dynamics study. *Chemical Physics Letters* **2009,** *468* (4), 260-263.

View Article Online
DOI: 10.1039/C8SM02301H
Second Revision – SM-ART-11-2018-002301.R1

32. Krafft, M. P., Controlling phospholipid self-assembly and film properties using highly fluorinated components – Fluorinated monolayers, vesicles, emulsions and microbubbles. *Biochimie* **2012,** *94* (1), 11-25.

33. Lehmler, H. J.; Bummer, P. M., Mixing of perfluorinated carboxylic acids with dipalmitoylphosphatidylcholine. *Biochimica et Biophysica Acta (BBA) - Biomembranes* **2004,** *1664* (2), 141-149.

34. Xie, W.; Bothun, G. D.; Lehmler, H.-J., Partitioning of perfluorooctanoate into phosphatidylcholine bilayers is chain length-independent. *Chemistry and Physics of Lipids* **2010,** *163* (3), 300-308.

35. Viada, B. N.; Juárez, A. V.; Pachón Gómez, E. M.; Fernández, M. A.; Yudi, L. M., Determination of the critical micellar concentration of perfluorinated surfactants by cyclic voltammetry at liquid/liquid interfaces. *Electrochimica Acta* **2018,** *263*, 499-507.

36. Wilke, N., Chapter Two - Lipid Monolayers at the Air–Water Interface: A Tool for Understanding Electrostatic Interactions and Rheology in Biomembranes. In *Advances in Planar Lipid Bilayers and Liposomes*, Aleš, I.; Chandrashekhar, V. K., Eds. Academic Press: 2014; Vol. Volume 20, pp 51-81.

37. Mercado, F. V.; Maggio, B.; Wilke, N., Phase diagram of mixed monolayers of stearic acid and dimyristoylphosphatidylcholine. Effect of the acid ionization. *Chemistry and Physics of Lipids* **2011,** *164* (5), 386-392.

38. Giudice, F.; Ambroggio, E. E.; Mottola, M.; Fanani, M. L., The amphiphilic alkyl ester derivatives of l-ascorbic acid induce reorganization of phospholipid vesicles. *Biochimica et Biophysica Acta (BBA) - Biomembranes* **2016,** *1858* (9), 2132-2139.

39. Brasitus, T. A.; Dudeja, P. K.; Worman, H. J.; Foster, E. S., The lipid fluidity of rat colonic brush-border membrane vesicles modulates Na+-H+ exchange and osmotic water permeability. *Biochimica et Biophysica Acta (BBA) - Biomembranes* **1986,** *855* (1), 16-24.

View Article Online
DOI: 10.1039/C8SM02301H
Second Revision – SM-ART-11-2018-002301.R1

40. Tocanne, J.-F.; Teissié, J., Ionization of phospholipids and phospholipid-supported interfacial lateral diffusion of protons in membrane model systems. *Biochimica et Biophysica Acta (BBA) - Reviews on Biomembranes* **1990,** *1031* (1), 111-142.

41. Registry, A. f. T. S. a. D., Toxic Substances Portal - Perfluoroalkyls. Atlanta. US.

42. George L. Gaines, J., Insoluble Monolayers at liquid-gas interfaces. John Wiley & Sons, I., Ed. New York 1966; pp 151-154.

43. Cámara, C. I.; Riva, J. S.; Juárez, A. V.; Yudi, L. M., Interaction of chitosan and self-assembled distearoylphosphatidic acid molecules at liquid/liquid and air/water interfaces. Effect of temperature. *J Phys Org Chem* **2016,** *29* (11), 672-681.

44. Cámara, C. I.; Wilke, N., Interaction of dextran derivatives with lipid monolayers and the consequential modulation of the film properties. *Chemistry and Physics of Lipids* **2017,** *204*, 34-42.

45. Matsumoto, Y.; Nakahara, H.; Moroi, Y.; Shibata, O., Langmuir Monolayer Properties of Perfluorinated Double Long-Chain Salts with Divalent Counterions of Separate Electric Charge at the Air−Water Interface. *Langmuir* **2007,** *23* (19), 9629-9640.

46. Bos, M. A.; Nylander, T., Interaction between β-Lactoglobulin and Phospholipids at the Air/Water Interface. *Langmuir* **1996,** *12* (11), 2791-2797.

47. de Matos Alves Pinto, L.; Malheiros, S. V. P.; Lino, A. C. S.; de Paula, E.; Perillo, M. A., Hydroxyzine, promethazine and thioridazine interaction with phospholipid monomolecular layers at the air-water interface. *Biophys Chem* **2006,** *119* (3), 247-255.

48. Elderdfi, M.; Sikorski, A. F., Langmuir-monolayer methodologies for characterizing protein-lipid interactions. *Chemistry and Physics of Lipids* **2018,** *212*, 61-72.

49. Stillwell, W., In *An Introduction to Biological Membranes (Second Edition)*, Stillwell, W., Ed. Elsevier: 2016.

50. Demel, R. A.; Geurts van Kessel, W. S. M.; Zwaal, R. F. A.; Roelofsen, B.; van Deenen, L. L. M., Relation between various phospholipase actions on human red cell membranes and the interfacial

View Article Online
DOI: 10.1039/C8SM02301H
Second Revision – SM-ART-11-2018-002301.R1

phospholipid pressure in monolayers. *Biochimica et Biophysica Acta (BBA) - Biomembranes* **1975,** *406* (1), 97-107.

51. Jähnig, F., What is the surface tension of a lipid bilayer membrane? *Biophysical Journal* **1996,** *71* (3), 1348-1349.

52. Stano, P.; Bufali, S.; Domazou, A. S.; Luisi, P. L., Effect of Tryptophan Oligopeptides on the Size Distribution of POPC Liposomes: A Dynamic Light Scattering and Turbidimetric Study. *Journal of Liposome Research* **2005,** *15* (1-2), 29-47.

53. Hulakova, S.; Fulier, B.; Gallova, J.; Balgavy, P., Effect of N-dodecyl-N,N-dimethylamine N-oxide on unilamellar liposomes. *Acta Facultatis Pharmaceuticae Universitatis Comenianae* **2013,** *60* (2), 7-13.

54. Kuzmin, P. I.; Akimov, S. A.; Chizmadzhev, Y. A.; Zimmerberg, J.; Cohen, F. S., Line Tension and Interaction Energies of Membrane Rafts Calculated from Lipid Splay and Tilt. *Biophysical Journal* **2005,** *88* (2), 1120-1133.

55. Dupuy, F.; Maggio, B., The hydrophobic mismatch determines the miscibility of ceramides in lipid monolayers. *Chemistry and Physics of Lipids* **2012,** *165* (6), 615-629.

56. Sánchez-Martín, M. J.; Haro, I.; Alsina, M. A.; Busquets, M. A.; Pujol, M., A Langmuir Monolayer Study of the Interaction of E1(145−162) Hepatitis G Virus Peptide with Phospholipid Membranes. *The Journal of Physical Chemistry B* **2010,** *114* (1), 448-456.

View Article Online
DOI: 10.1039/C8SM02301H
Second Revision – SM-ART-11-2018-002301.R1

(a) DSPA

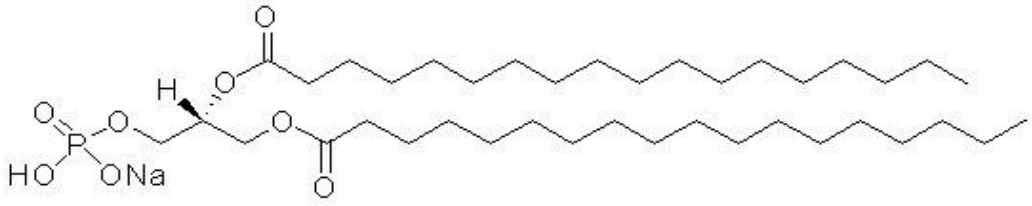

(b) DSPE

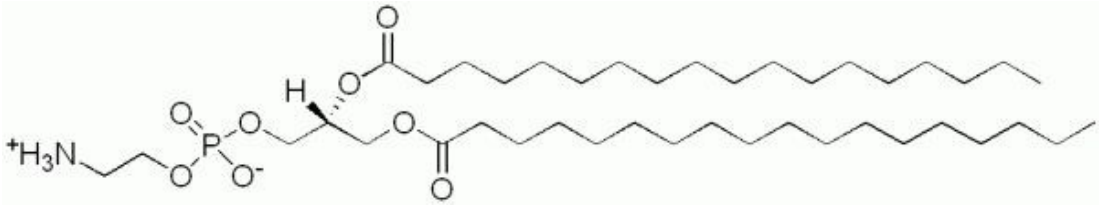

(c) DLPA

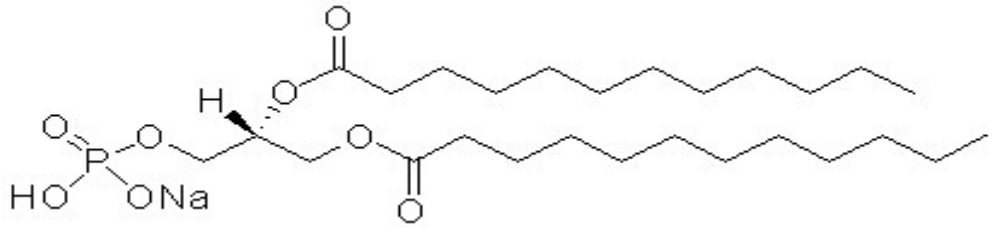

(d) PFD

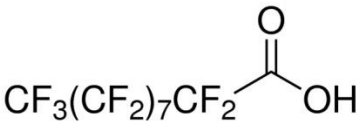

Figure 1: Structures of; **(a)** 1,2- disteraroyl-*sn*- glycerol-3-phosphate, **(b)** 1,2- disteraroyl-*sn*- glycerol-3-phosphoetanolamine **(c)** 1,2- dilauroyl-*sn*- glycerol-3-phosphate, and **(d)** perfluorodecanoic acid**.**

View Article Online
DOI: 10.1039/C8SM02301H
Second Revision – SM-ART-11-2018-002301.R1

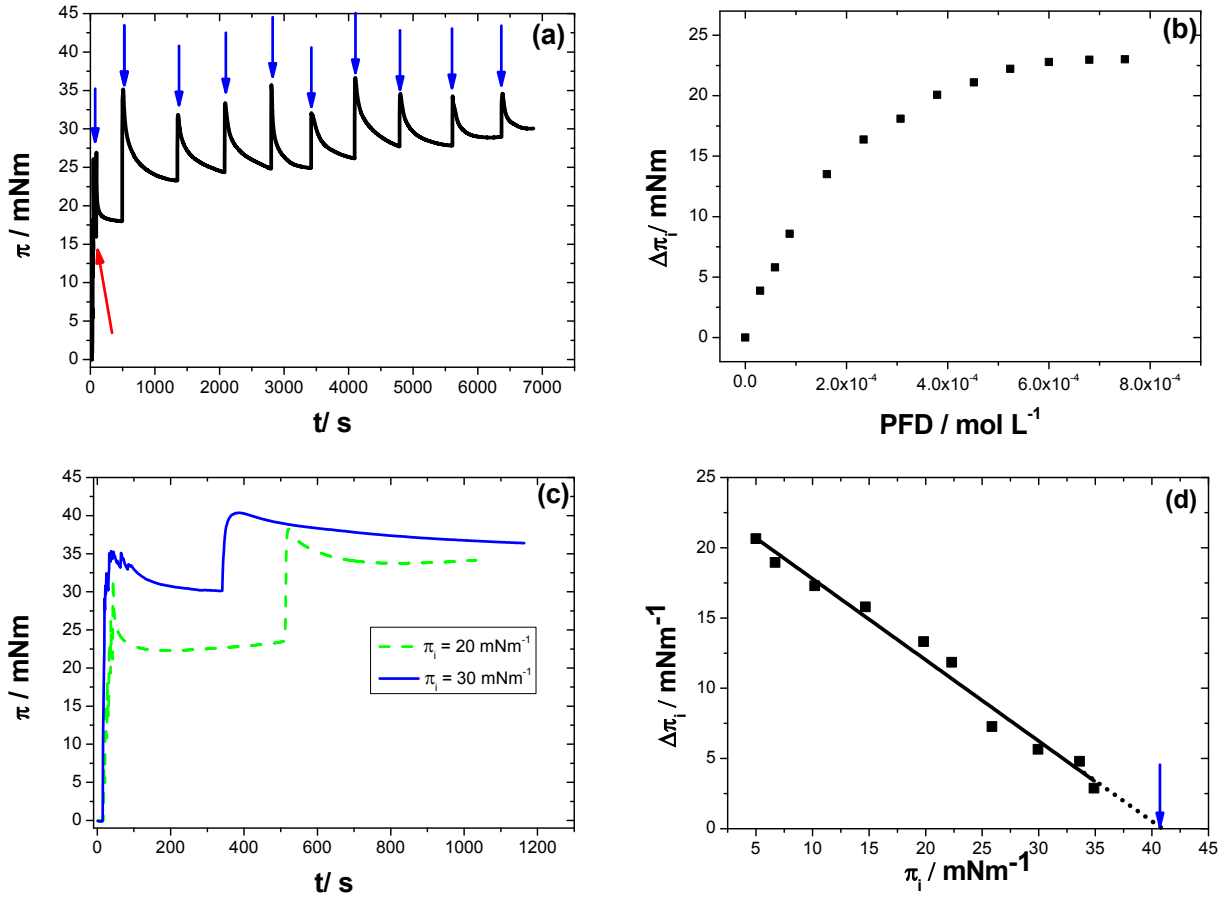

Figure 2: Typical sequence for the determination of exclusion pressure of PFD from the lipid monolayer using the constant surface-area approach: a) successive injections of PFA on a pre-formed DSPE monolayer at initial pressure of 15 mN, b) change in surface pressure with respect to initial pressure at each PFD concentration calculated from Figure 2 a), c) surface pressure variation before and after the injection of PFD at a concentration equal to saturation value observed in Figure 2 b) for two different initial surface pressures, d) plot of $\Delta\pi$ values obtained from figure 2 c) as a function of initial pressure.

View Article Online
DOI: 10.1039/C8SM02301H
Second Revision – SM-ART-11-2018-002301.R1

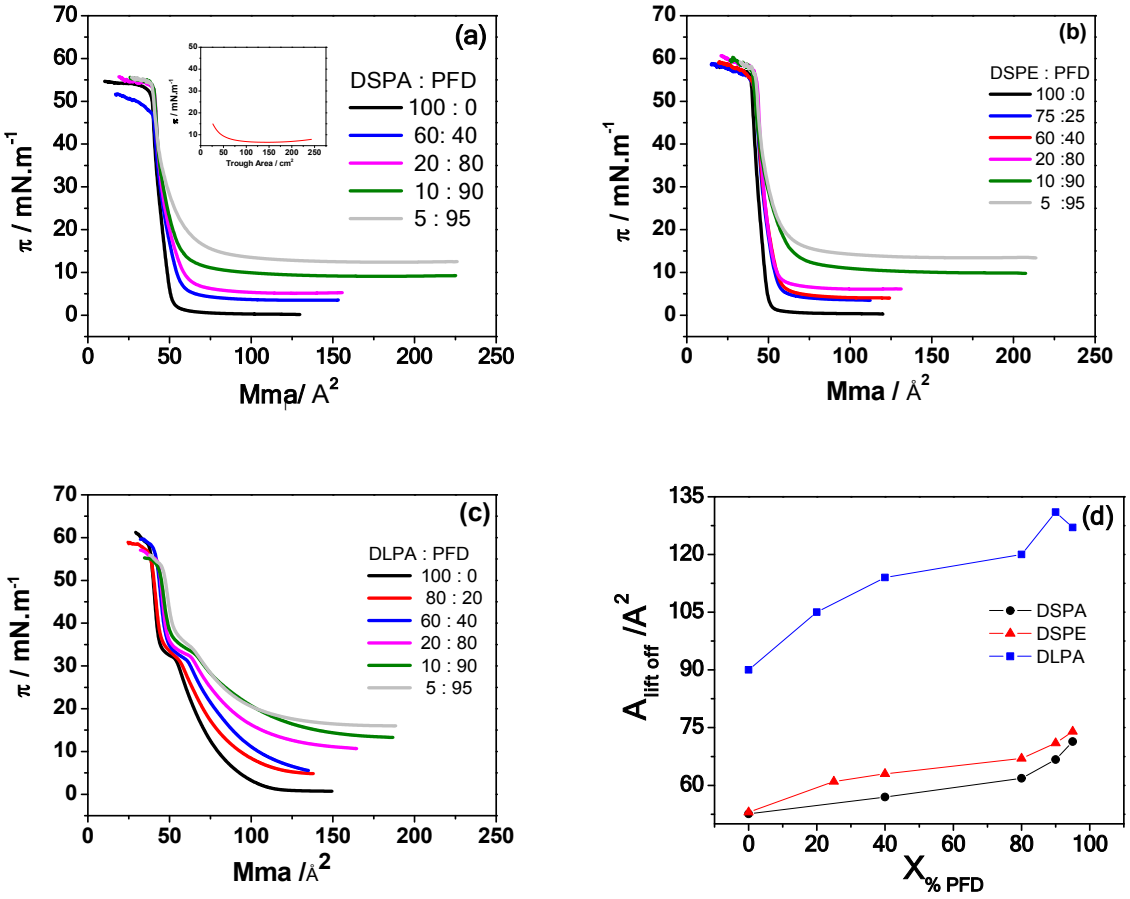

Figure 3: Surface pressure - average molecular area (Mma/Å²) compression isotherms for the mixtures: **(a)** DSPA:PFD; inset: PFD: 100 %, **(b)** DSPE:PFD, **(c)** DLPA:PFD, at molar fractions Lipid:PFD 100:0 **(black)**, 80:20 (**red**), 60:40 (**blue**), 20:80 (**magenta**), 10:90 (**green**) and 5:95 (**gray**). **(d)** Lift-off areas as a function of PFD molar fraction for: DSPE (**red**), DSPA (**Black**) and DLPA (**blue**). Experimental conditions for the subphase: 10 mM LiCl, pH = 6.00 and T = 21°C.

View Article Online
DOI: 10.1039/C8SM02301H
Second Revision – SM-ART-11-2018-002301.R1

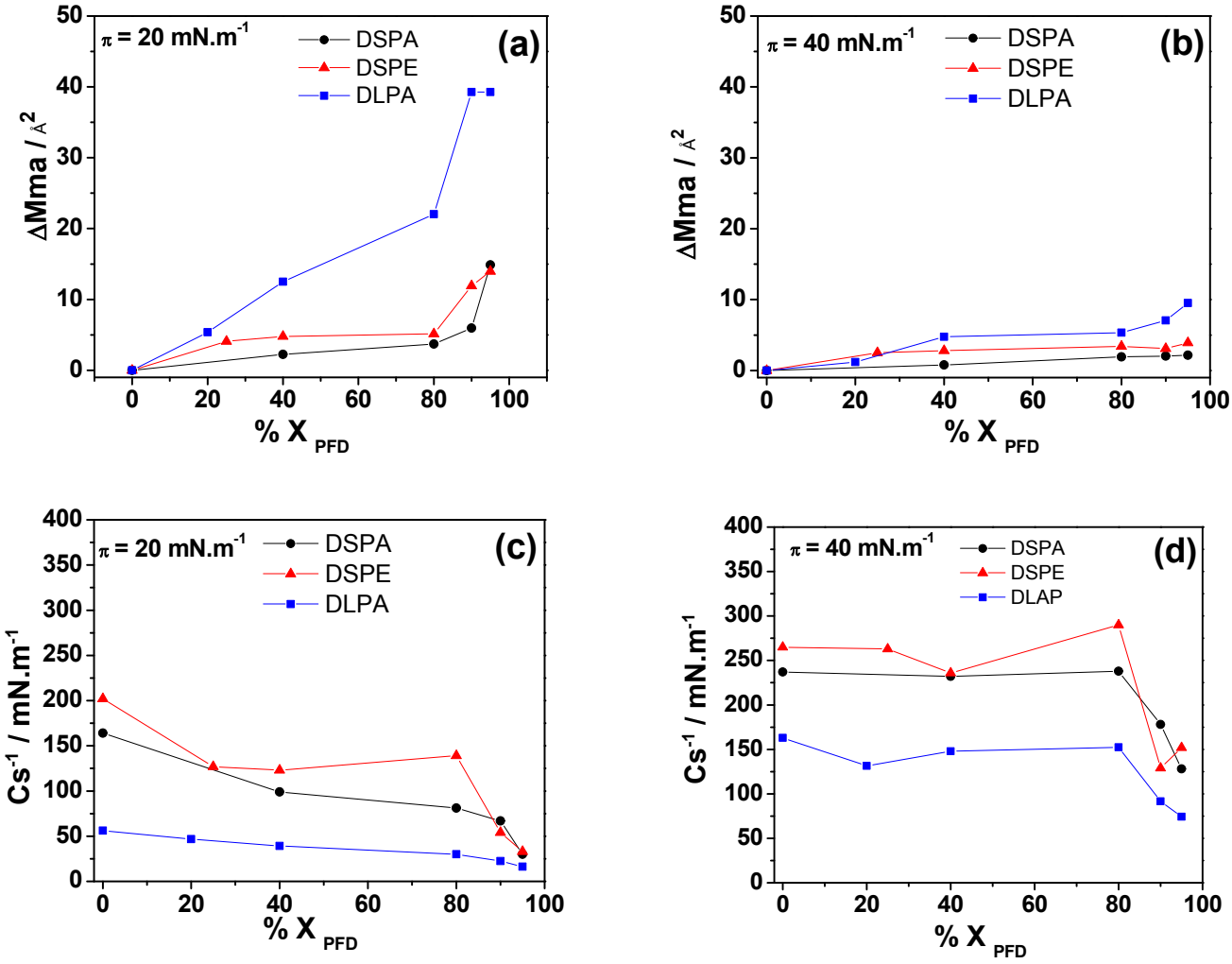

Figure 4: (**a-b**) Change of mean molecular area (ΔMma = Mma $_{X\ PFD}$ – Mma $_{pure\ lipid}$) and (**c-d**) compressibility factor as a function of PFD molar fraction (X_{PFD}) at 20 mN.m^{-1} **(a-c)** or 40 mN.m^{-1} **(b-d),** for DSPA:PFD (**black**), DSPE:PFD (**red**) and DLPA:PFD (**blue**) mixtures. Experimental conditions for the subphase: 10 mM LiCl, pH = 6.00 and T = 21°C.

View Article Online
DOI: 10.1039/C8SM02301H
Second Revision – SM-ART-11-2018-002301.R1

DSPA: PFD

(a) 100: 0

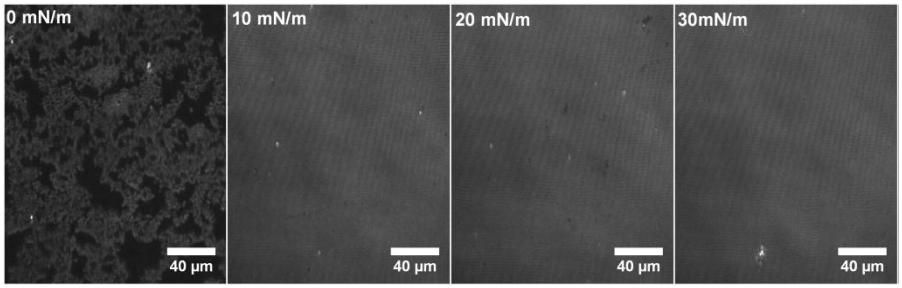

(b) 60: 40

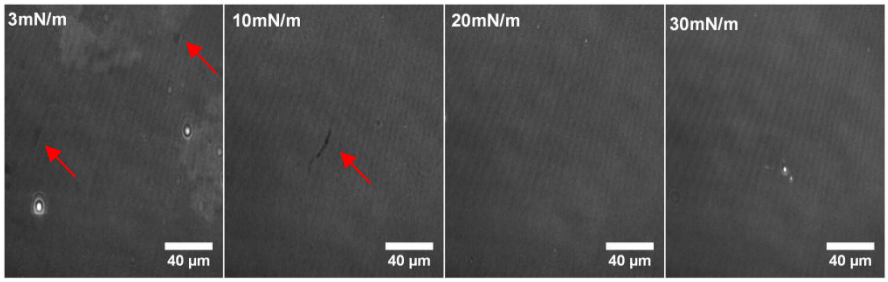

(c) 10:90

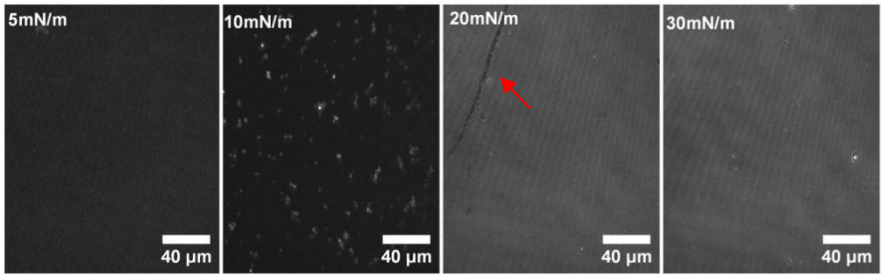

Figure 5: BAM images for DSPA:PFD monolayers at the ratios: **(a)** 100:0, **(b)** 60:40 and **(c)** 10:90 and different surface pressures, from 0 to 30 mNm^{-1}. The gray levels were rescaled from the original range 0-255 to 0-130 for better visualization. Experimental conditions for the subphase: 10 mM LiCl, pH = 6.00 and T = 21°C.

View Article Online
DOI: 10.1039/C8SM02301H
Second Revision – SM-ART-11-2018-002301.R1

DSPE:PFD

(a) 100: 0

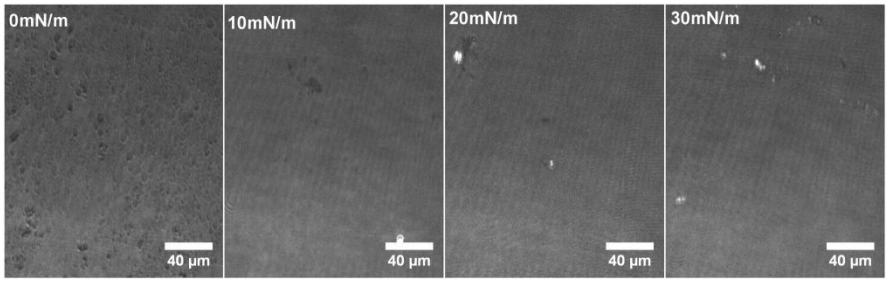

(b) 60: 40

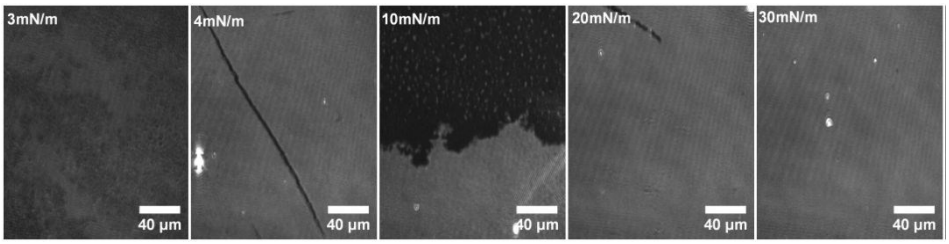

(c) 10: 90

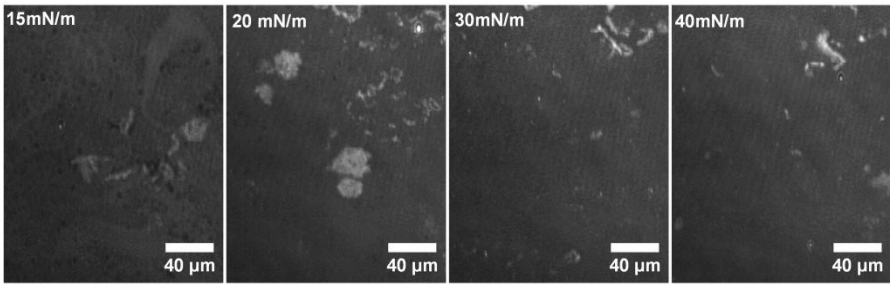

Figure 6: BAM images for DSPE:PFD monolayers at the ratios: **(a)** 100:0, **(b)** 60:40 and **(c)** 10:90 and different surface pressures, from 0 to 40 mNm^{-1}.The gray levels were rescaled from the original range 0-255 to 0-130. Experimental conditions for the subphase: 10 mM LiCl, pH = 6.00 and T = 21°C.

View Article Online
DOI: 10.1039/C8SM02301H
Second Revision – SM-ART-11-2018-002301.R1

DLPA: PFD

(a) 100: 0

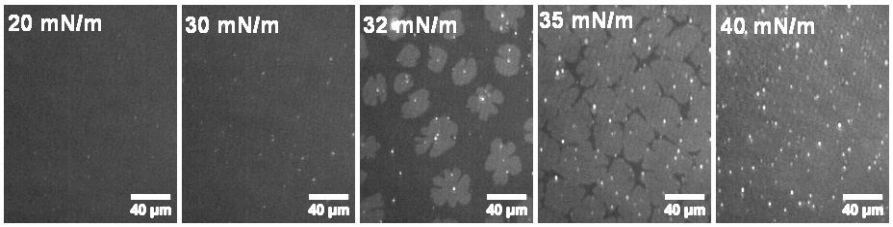

(b) 60:40

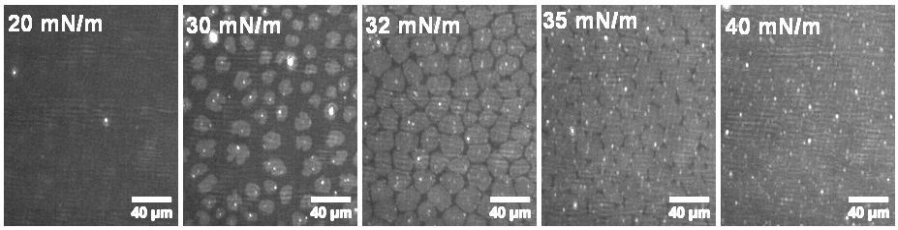

(c) 10:90

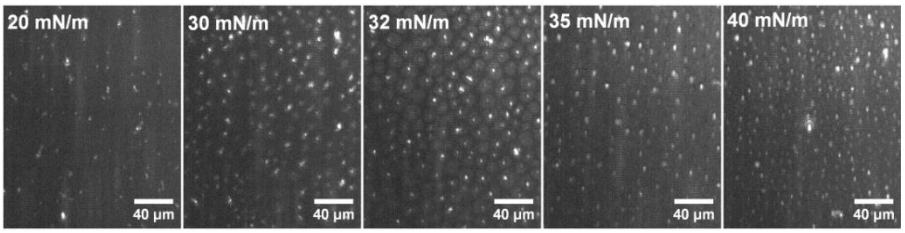

Figure 7: BAM images for DLPA:PFD monolayers at the ratios: **(a)** 100:0, **(b)** 60:40 and **(c)** 10:90 and different surface pressures, from 0 to 40 mNm^{-1}. The gray levels were rescaled from the original range 0-255 to 6 -42 for better visualization. Experimental conditions for the subphase: 10 mM LiCl, pH = 6.00 and T = 21°C.

View Article Online
DOI: 10.1039/C8SM02301H
Second Revision – SM-ART-11-2018-002301.R1

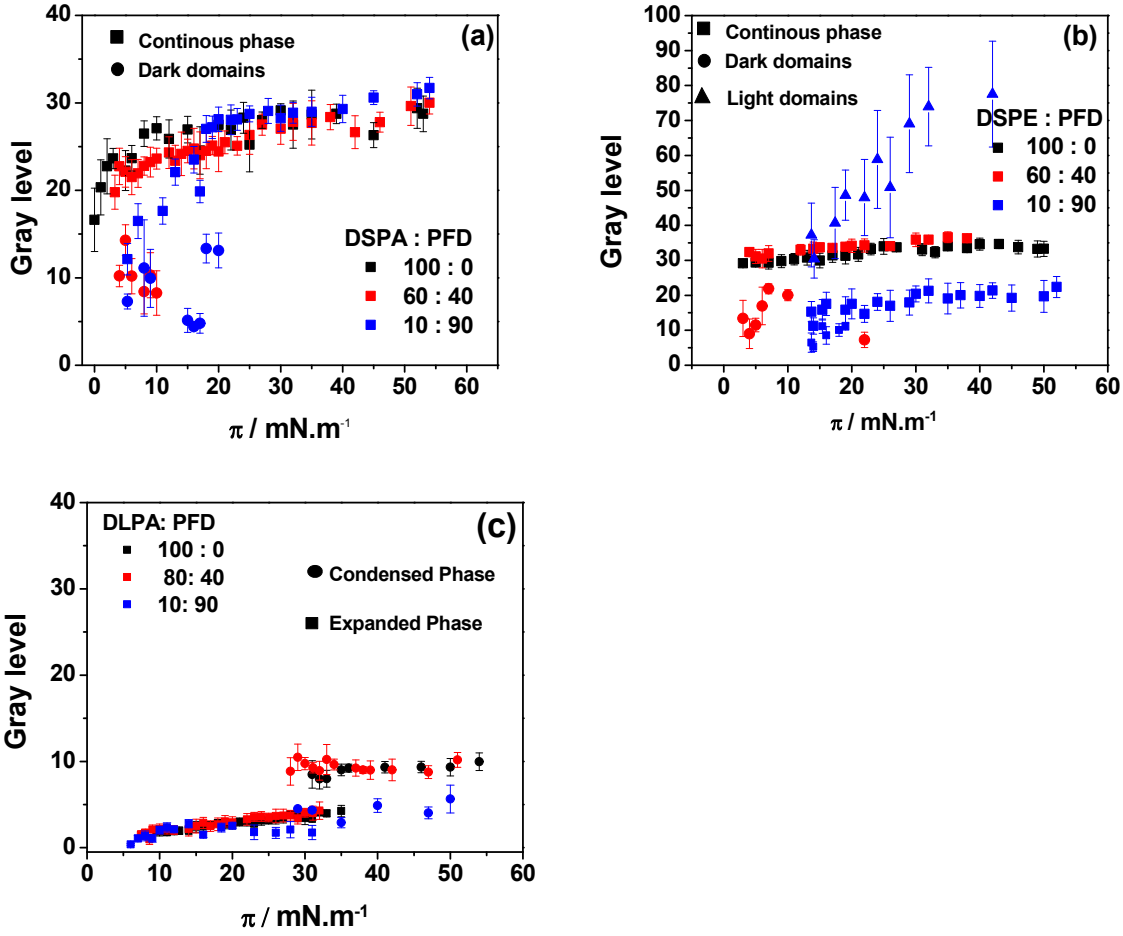

Figure 8: Average gray level (± standard deviation) as a function of surface pressure for **(a)** DSPA:PFD, **(b)** DSPE:PFD and **(c)** DLPA:PFD monolayers. Lipid: PFD ratios: 100:0 (**black**), 60: 40 (**red**) and 10:90 (**blue**). Experimental conditions for the subphase: 10 mM LiCl, pH = 6.00 and T = 21°. **(a-b) circle:** dark domains, **square:** continues phase and **triangle:** light domains; **(c) square:** expanded phase and **circle:** condensed phase.

View Article Online
DOI: 10.1039/C8SM02301H
Second Revision – SM-ART-11-2018-002301.R1

(a)

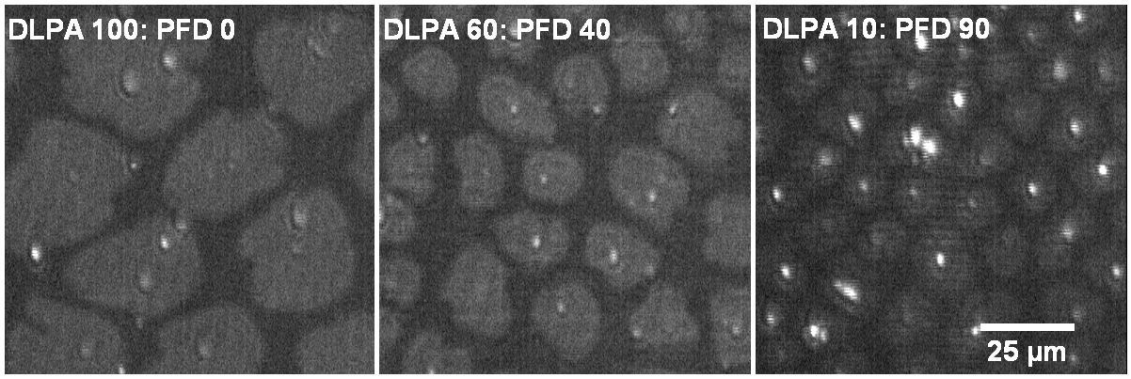

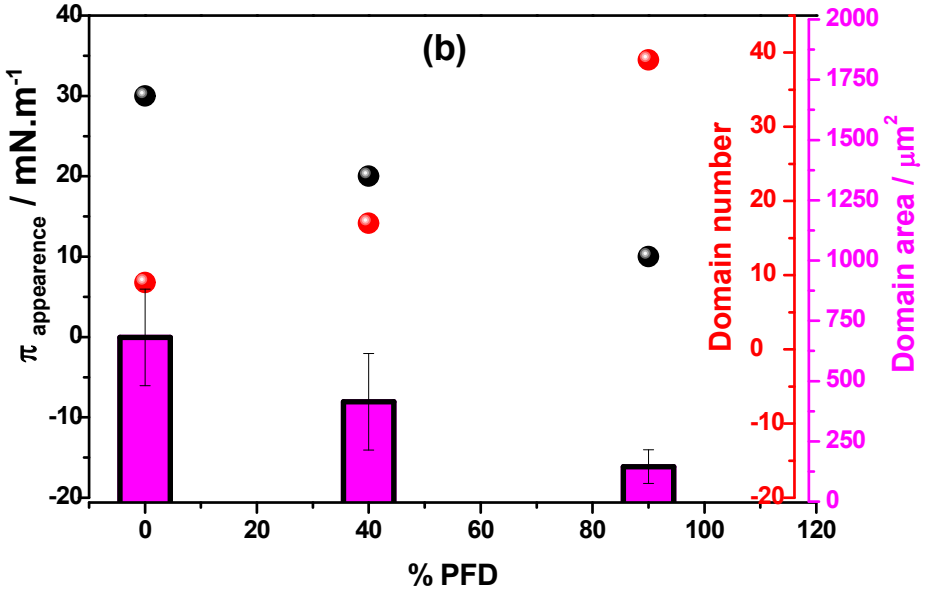

Figure 9: (a) Brewster angle images for DLPA:PFD mixtures, obtained at the 60 % of the phase transition. (Surface pressures: 31 mN.m^{-1} for ratio 100:0, 30,7 mN.m^{-1} for ratio 60:40, 30 mN.m^{-1} for ratio 10:90) Size: *100 µm² x 100 µm²*, the images were rescale from the original range 0-255 to 6-42 for better visualization. **(b)** Surface pressure of domain appearance, domain numbers and areas as a function of PFD molar fraction for DLPA:PFD mixtures, obtained from images shown on **(a)**.

View Article Online
DOI: 10.1039/C8SM02301H
Second Revision – SM-ART-11-2018-002301.R1

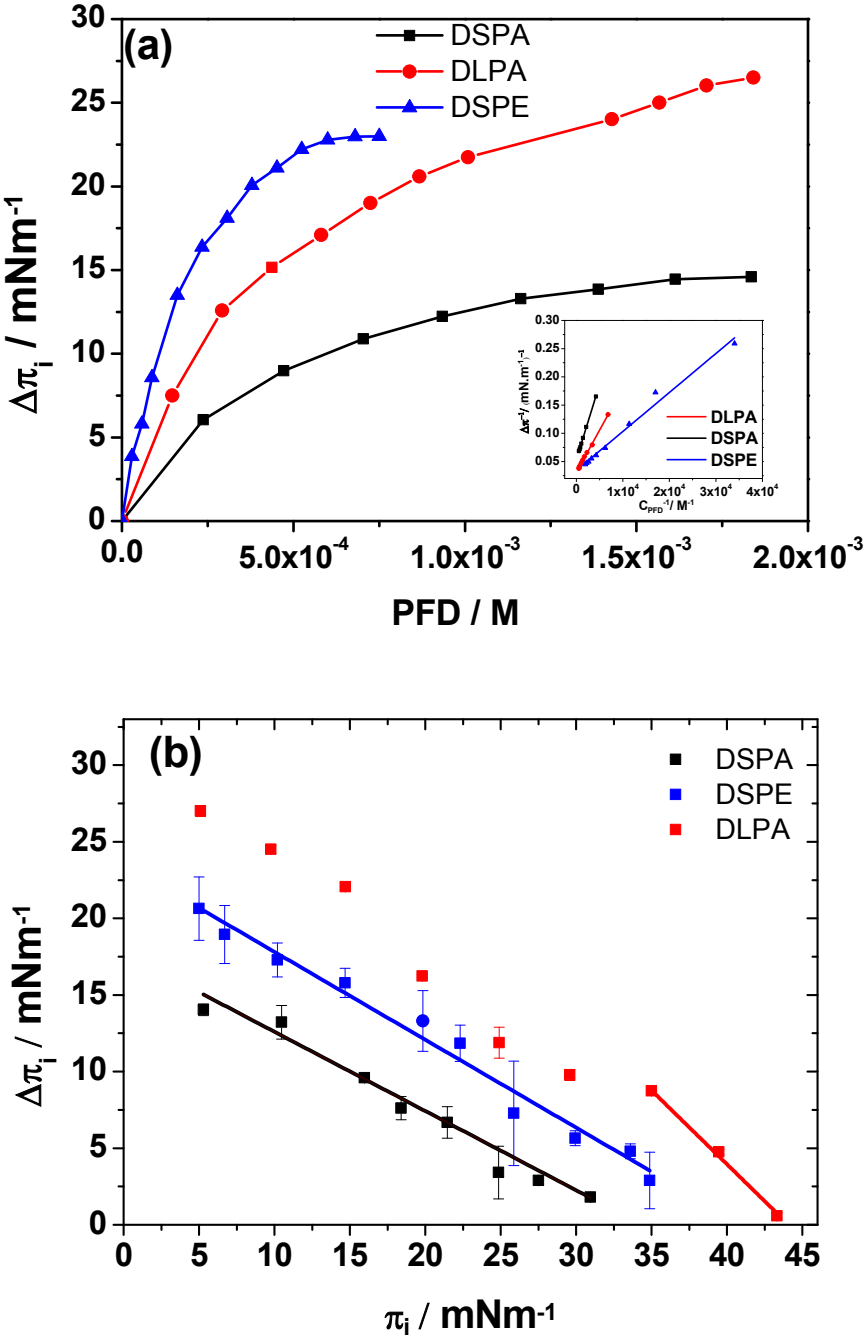

Figure 10: (a) Δπ vs PFD concentration in the subphase (adsorption isotherm). Inset: adsorption isotherm linearization. **(b)** Δπ (Δπ = $\pi_{t= 30\ min}$ - $\pi_{t= 0\ min}$) as a function of the initial pressure, for DSPA (**black**), DSPE (**blue**) and DLPA (**red**) monolayers in the presence of PFD in the subphase. Experimental conditions for the subphase: 10 mM LiCl, x M PFD, pH = 6.00 and T = 21°C.

View Article Online
DOI: 10.1039/C8SM02301H
Second Revision – SM-ART-11-2018-002301.R1

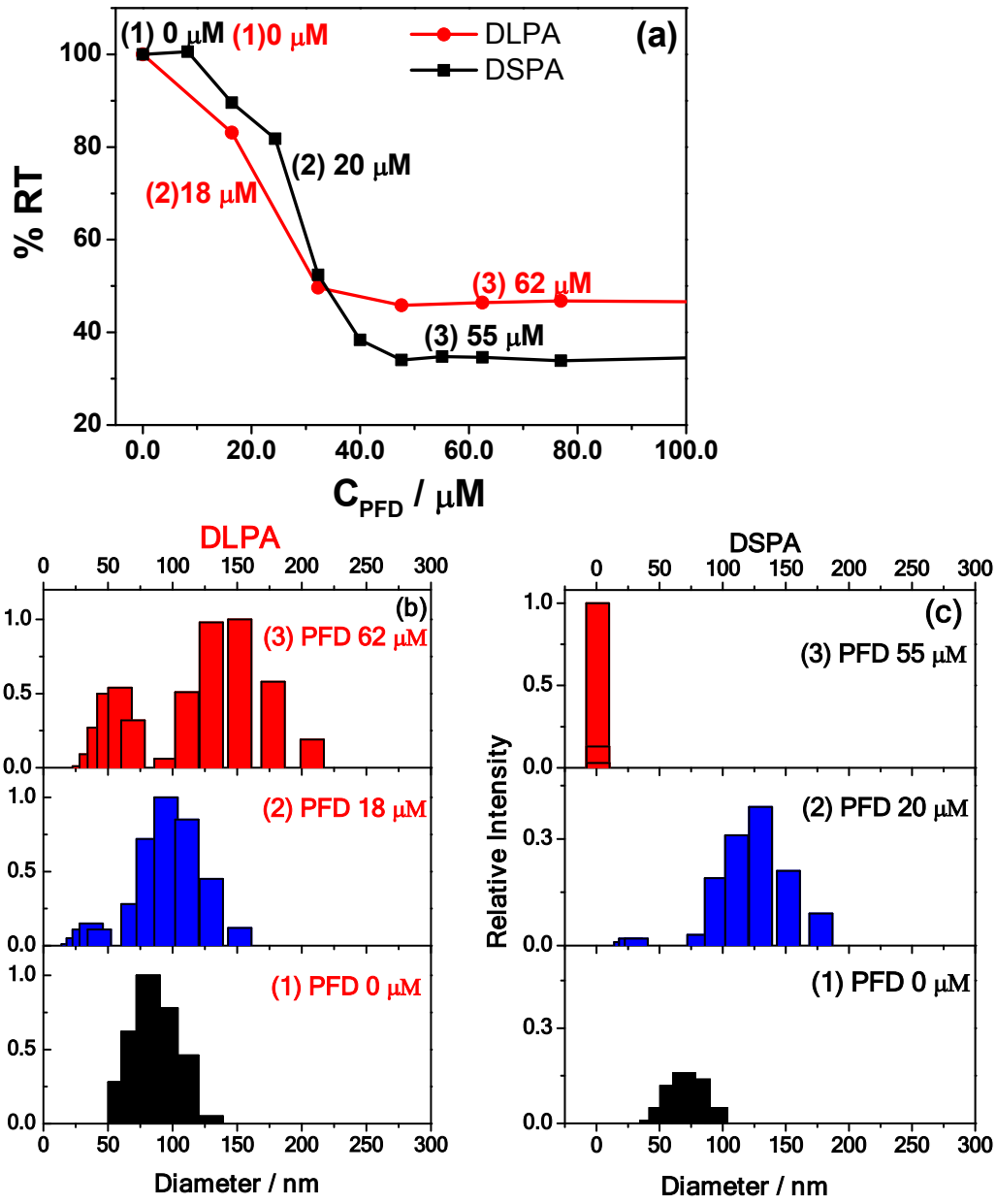

Figure 11: (a) Percent of relative turbidity (%RT) vs PFD concentration for LUVs of DSPA (**black**) and DLPA (**red**) in LiCl 10mM. **(b and c)** Relative frequency (intensity) as function of LUV diameter for DLPA **(b)** and DSPA **(c)** LUVs in absence (black) and in the presence of PFD blue and red). Subphase composition: LiCl 10 mM.

View Article Online
DOI: 10.1039/C8SM02301H
Second Revision – SM-ART-11-2018-002301.R1

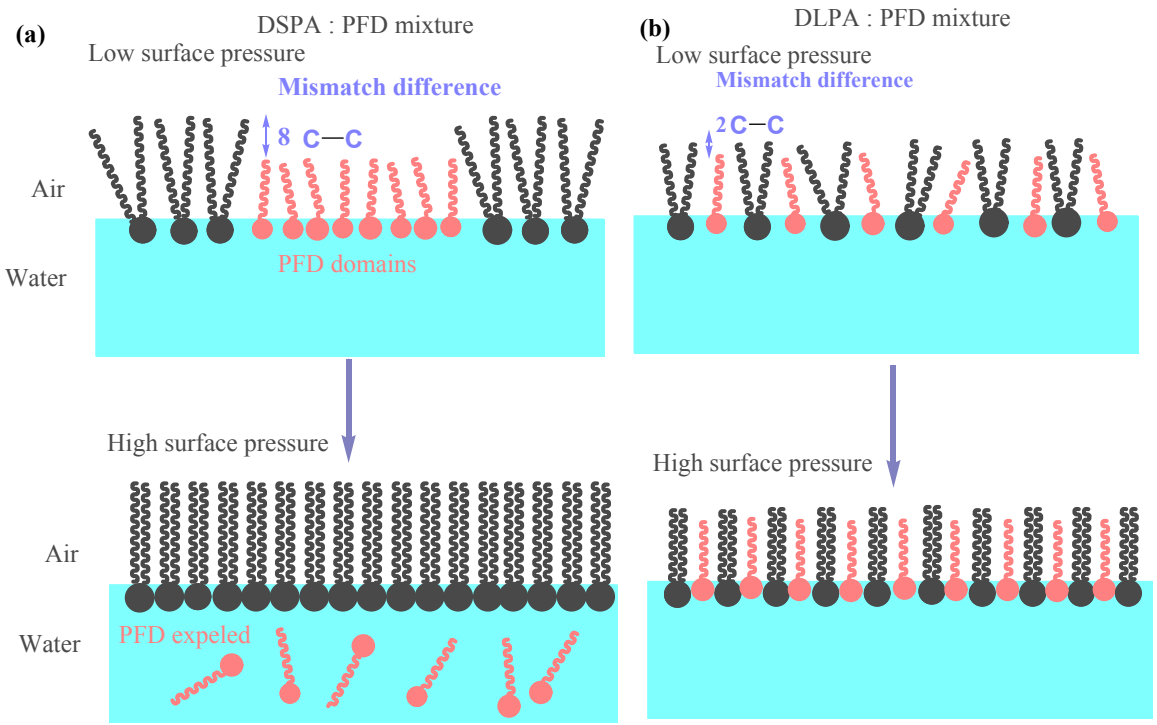

Figure 12: Proposed model for lipid:PFD interaction for **(a)** DSPA:PFD (60:40), immiscible system and **(b)** DLPA: PFD mixtures, miscible sytem; **upper image** correspond to low surface pressures and **lower image** correspond to the mixtures at high surface pressures.

View Article Online
DOI: 10.1039/C8SM02301H
Second Revision – SM-ART-11-2018-002301.R1

Table 1: Saturation Concentration (SC); Maximum change in surface pressure ($\Delta\pi_{max}$); constant $K_{0.5}$ and Exclusion pressure values for DSPA, DSPE and DLPA in the presence of PFD.

Phospholipid	SC / mM	$\Delta\pi_{max}$ / mN.m^{-1}	$K_{0.5}$ /mM	Exclusion Pressure value /mN.m^{-1}
DSPA	1.7	(18.8 ± 0.2)	(0.50±0.02)	(34.2±0.9)
DSPE	0.52	(29 ± 3)	(0.200±0.007)	(41±2)
DLPA	1.6	(33± 3)	(0.48±0.2)	(44±2)*

*** The value was obtained from the linear fitting carried out with $\Delta\pi$ values corresponding to the condensed phase, see Figure 10.**

View Article Online
DOI: 10.1039/C8SM02301H

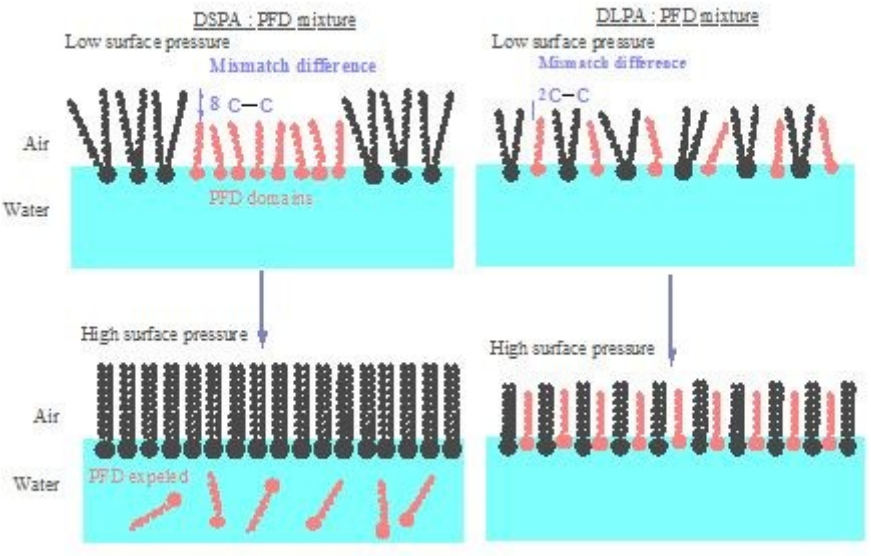

The surfactant perfluorodecanoic acid (PFD), widely used in different industrial applications and an important environmental contaminant, can penetrate distearoyl phosphatidic acid (DSPA), dilauroyl phosphatidic acid (DLPA) and distearoyl phosphatidylethanolamine (DSPE) monolayers, even at high pressures values, above 30 mNm^{-1}, which is the lateral pressure value accepted for cellular bilayer.